



HAL
open science

Impairment of the cellulose degradation machinery enhances *Fusarium oxysporum* virulence but limits its reproductive fitness

Francisco Gámez-Arjona, Stefania Vitale, Aline Voxeur, Susanne Dora, Sascha Müller, Gloria Sancho-Andrés, Juan Carlos Montesinos, Antonio Di Pietro, Clara Sánchez-Rodríguez

► To cite this version:

Francisco Gámez-Arjona, Stefania Vitale, Aline Voxeur, Susanne Dora, Sascha Müller, et al.. Impairment of the cellulose degradation machinery enhances *Fusarium oxysporum* virulence but limits its reproductive fitness. *Science Advances* , 2022, 8 (16), pp.eabl9734. 10.1126/sciadv.abl9734 . hal-03752595

HAL Id: hal-03752595

<https://hal.inrae.fr/hal-03752595>

Submitted on 10 Jan 2024

HAL is a multi-disciplinary open access archive for the deposit and dissemination of scientific research documents, whether they are published or not. The documents may come from teaching and research institutions in France or abroad, or from public or private research centers.

L'archive ouverte pluridisciplinaire **HAL**, est destinée au dépôt et à la diffusion de documents scientifiques de niveau recherche, publiés ou non, émanant des établissements d'enseignement et de recherche français ou étrangers, des laboratoires publics ou privés.





Distributed under a Creative Commons Attribution - NonCommercial 4.0 International License

Impairment of the cellulose degradation machinery enhances *Fusarium oxysporum* virulence but limits its reproductive fitness

Journal Article

Author(s):

Gámez-Arjona, Francisco; Vitale, Stefania; Voxeur, Aline; Dora, Susanne; Müller, Sascha; [Sancho Andrés, Gloria](#) ; [Montesinos Lopez, Juan Carlos](#) ; Di Pietro, Antonio; Sánchez-Rodríguez, Clara

Publication date:

2022-04

Permanent link:

<https://doi.org/10.3929/ethz-b-000544950>

Rights / license:

[Creative Commons Attribution-NonCommercial 4.0 International](#)

Originally published in:

Science Advances 8(16), <https://doi.org/10.1126/sciadv.abl9734>

Funding acknowledgement:

184769 - Understanding the molecular biology of plant - vascular pathogen interaction (SNF)

MICROBIOLOGY

Impairment of the cellulose degradation machinery enhances *Fusarium oxysporum* virulence but limits its reproductive fitness

Francisco M. Gámez-Arjona¹, Stefania Vitale^{2†}, Aline Voxel³, Susanne Dora¹, Sascha Müller¹, Gloria Sancho-Andrés¹, Juan Carlos Montesinos¹, Antonio Di Pietro², Clara Sánchez-Rodríguez^{1*}

Fungal pathogens grow in the apoplastic space, in constant contact with the plant cell wall (CW) that hinders microbe progression while representing a source of nutrients. Although numerous fungal CW modifying proteins have been identified, their role during host colonization remains underexplored. Here, we show that the root-infecting plant pathogen *Fusarium oxysporum* (Fo) does not require its complete arsenal of cellulases to infect the host plant. Quite the opposite: Fo mutants impaired in cellulose degradation become hypervirulent by enhancing the secretion of virulence factors. On the other hand, the reduction in cellulase activity had a severe negative effect on saprophytic growth and microconidia production during the final stages of the Fo infection cycle. These findings enhance our understanding of the function of plant CW degradation on the outcome of host-microbe interactions and reveal an unexpected role of cellulose degradation in a pathogen's reproductive success.

INTRODUCTION

Most plant-microbe interactions are initially established at the apoplast. Here, the plant cell wall (CW) constitutes not only a physical barrier but also a potential important source of nutrients for the intruder, making its modification an important aspect of microbe colonization of the host. The main components of plant CWs are the paracrystalline fibers of cellulose embedded in a matrix of hemicellulose, pectin, lignin, and suberin (1–3). Ions and wall remodeling proteins modify the interactions between CW polysaccharides in muro, changing the physicochemical properties and, consequently, the structure and function of the CW (4, 5). The CW composition is not homogeneous among different plant species and tissues or even within a single cell (6). This molecular complexity forces plant-colonizing microbes to metabolically regulate the secretion of a broad set of CW modifying proteins (CWMPs) required to loosen and digest the plant CWs they encounter (7, 8). Most of these CWMPs are CW degrading enzymes (CWDEs), including glycosyl hydrolases, lytic polysaccharide monoxygenases, pectate and pectin lyases, and esterases, which are further divided into different subgroups based on sequence similarity in the catalytic domain (9–12). Although some plant-colonizing fungi have a low number of CWMPs and benefit from the host CW degrading machinery to infect (13, 14), plant fungal pathogens generally encode for a high number of CWMPs, whose expression seems to be essential during host infection (15–18). However, so far, the large functional redundancy of CWMPs has largely prevented a complete assessment of their role (19), since deletion of individual CWMP genes does not generally affect the virulence of the pathogen (20). Fungi have evolved transcription factors that co-regulate the expression of CWMP

groups based on the composition of their environment. Therefore, it has been suggested that targeting such master transcriptional regulators should allow the assessment of the role of a given group of CWMPs (21).

During plant-microbe coevolution, the intruders adapted to loosen and break the host CWs, while the hosts evolved to perceive these degradation products as damage-associated molecular patterns (DAMPs). These DAMPs, together with microbe-associated molecular patterns (MAMPs) such as fungal chitin (22), activate the plant pattern-triggered immunity against the intruder (23, 24). The best characterized CW-derived DAMPs are pectin-derived oligogalacturonides (OGs), resulting from pectinase activity (25–27). Cellulose degradation products, i.e., like cellobiose, have also been shown to induce plant defense and are, therefore, considered potential DAMPs, although their release upon microbe colonization has not yet been proven (27, 28).

The plant CW characteristics directly influence communication between the two organisms. This is particularly relevant for plant response to microbes that mainly live in the apoplast, such as vascular fungi belonging to the *Fusarium oxysporum* (Fo) species complex, which are further classified into different formae speciales (ff.spp.) based on their host preference (29). Fo_s are soil-borne microbes that colonize the roots of many plant species, being responsible for the devastation of many economically important crops throughout the world (29). Fo_s are considered pathogenic when they cause plants to wilt and eventually die, which occurs because water flow and nutrient uptake are blocked by fungal proliferation inside the xylem. To reach the vascular system, Fo grows predominantly in the root apoplast (30, 31), making this fungus an ideal model to study CW-microbe interaction.

Cellulose is the most abundant and most recalcitrant component of the CW that provides mechanical strength to the plant cells because of its paracrystalline structure (7). Consequently, its synthesis is tightly regulated in response to intruders, including Fo (32–34), making cellulose one of the main targets of microbial CWMPs. Pathogens secrete a broad range of cellulolytic enzymes [glycosyl hydrolases (GHs) and lytic polysaccharide monoxygenases (AAs)]

¹Department of Biology, ETH Zurich, 8092 Zurich, Switzerland. ²Departamento de Genética, Campus de Excelencia Internacional Agroalimentario ceiA3, Universidad de Córdoba, 14014 Córdoba, Spain. ³Institut Jean-Pierre Bourgin, INRA, Centre National pour la Recherche Scientifique, AgroParisTech, Université Paris-Saclay, RD10, 78026 Versailles Cedex, France.

*Corresponding author. Email: clara_sanchez@ethz.ch

†Present address: IPSP-Instituto per la Protezione Sostenibile delle Piante, CNR, 80055 Portici, Italy.

(17), suggesting that this family of enzymes should be essential for infection. An optimal degradation of complex carbohydrates requires a hierarchical metabolic response. In the case of crystalline cellulose, AAs disrupt the outermost crystalline part of the cellulose fiber, thereby allowing the remaining cellulases to participate in the degradation process (9, 35, 36). The transcriptional regulation of fungal cellulases in ascomycetes has been reported to be dependent on a conserved cluster of zinc binuclear transcription factors in ascomycetes (7). Besides XlnR/XLR-1/Xyr1 (37), this cluster includes CLR1/ClrA that is required for growth on cellulose as the sole carbon source in many, albeit not all, fungi (38–40).

Here, we investigated the impact of cellulose degradation during microbe infection by identifying and targeting the orthologs of *Neurospora crassa* CLR1 in *Fo* f. sp. *conglutinans* (Fo5176) and *lycopersici* (Fol4287), pathogens of *Arabidopsis thaliana* and *Solanum lycopersicum*, respectively (41, 42). Unexpectedly, our data show that crystalline cellulose degradation is not indispensable for *Fo* infection, as shown by the increased virulence displayed by Δ *clr1* mutants. Using the model pathosystem *A. thaliana*–Fo5176 (33, 34, 43, 44), we show that the Δ *clr1* mutant compensates for cellulose degradation deficiency by increasing the secretion of various virulence factors to compromise plant immune responses. On the other hand, the reduction of cellulose degradation capacity severely compromised fungal metabolism during its saprophytic growth, with marked consequences for its microconidia production. Together, our findings expand the current understanding of plant-microbe interactions, showing that cellulose is not the assumed central physical barrier against *Fo* on their way toward the plant vasculature. Instead, we show that cellulose is a primary source of carbon in later time points of colonization and its degradation is necessary to complete their life cycle in the plant.

RESULTS

The transcriptional regulator CLR1 is required for efficient cellulose degradation by Fo5176

To understand the role of *Fo* cellulases in root infection, we aimed to obtain an Fo5176 mutant impaired in cellulose degradation. Considering the large number of putative cellulases expressed by Fo5176 during root colonization (34) and their high functional redundancy, we chose to target the transcription factor CLR1, a master regulator of fungal cellulase expression previously identified in *N. crassa* (38). Using an in silico analysis, we found CLR1 orthologs in various *Fusarium* genomes, sharing a protein sequence identity above 70% and having the exact same sequence as the DNA binding domain identified in *N. crassa* (Fig. 1, A and B) (39). Therefore, we generated a CLR1 null mutant in the previously described Fo5176 *pSIX1::GFP* background, which allows for monitoring Fo5176 colonization of the root vasculature (33, 44). We obtained deletion mutants lacking the entire CLR1 coding region (Δ *clr1-1* and Δ *clr1-2*) and a complemented strain (*clr1C*) generated by reintroducing the wild-type (WT) *pCLR1::CLR1* into the Δ *clr1-1* mutant background (fig. S1). We first determined whether the lack of CLR1 affected fungal growth, especially in conditions where its CW is challenged. Δ *clr1-1* was grown in control conditions [yeast extract, peptone, and dextrose (YPD)], salt stress (NaCl), osmotic stress (sorbitol), and CW stress (Congo red and Calcofluor) (45), as well as on minimal medium. There were no detectable differences in the colony phenotype of Δ *clr1* mutants compared to WT in any of these conditions

(fig. S2). Next, we evaluated the role of CLR1 in cellulose degradation by *Fo* by testing the ability of Δ *clr1-1*, *clr1C*, and WT to use different carbon sources such as sucrose, cellobiose, and cellulose. Fungal growth on sucrose was similar across all genotypes (Fig. 1, C and D, and fig. S3). The Δ *clr1-1* mutant exhibited a significant growth reduction on cellobiose and only showed residual growth on cellulose compared to WT or *clr1C* (Fig. 1, C and D, and fig. S3). A similar phenotype was observed for Δ *clr1-2* (fig. S4, A and B). These data are similar to those described in *N. crassa* (38), indicating that the essential function of CLR1 in cellulose catabolism is conserved between *N. crassa* and *Fo*.

Loss of CLR1 leads to faster colonization of the root cortex and xylem

To determine whether *Fo* requires cellulose degradation to infect its plant hosts, we performed plate infection assays as described before (44). We monitored root vascular colonization by following green fluorescent protein (GFP) signal presence in the root vasculature at different days post-transfer (dpt) to spore-containing plates. Unexpectedly, we counted a significantly higher number of vascular penetrations of Δ *clr1-1* than WT and *clr1C* at all time points, correlated with a higher activity of the promoter quantified through expression of *FoSIX1* (46), and an increased in planta fungal biomass at 7 dpt measured by quantitative reverse transcription polymerase chain reaction (PCR) (Fig. 2, A to D). A second isogenic mutant, Δ *clr1-2*, also showed a higher capacity than WT to reach the host xylem (fig. S4C). We therefore focused on the Δ *clr1-1* mutant for further characterization. Using confocal microscopy, we observed that Δ *clr1-1* advanced faster than WT and *clr1C* through the epidermal apoplast as it could be seen in the epidermis-cortex interface at 3 dpt with a significant higher frequency than the WT fungus (Fig. 2, E and F). These results indicate that Δ *clr1-1* is more efficient than WT in growing through the host CWs and reaching the xylem, and might explain the higher levels of vascular invasion observed at later stages of the infection (Fig. 2, A to C).

At 7 dpt, when the fungus is colonizing the vasculature in all roots, we observed a reduced expression of genes required for cellulose degradation in Δ *clr1-1* compared to WT including endoglucanase (g9160), glycosyl hydrolase family 5 member (g5102), and two AA9 enzymes (g17213 and g13080). We also detected significant changes in the expression of genes related with sugar metabolism such as a plasma membrane hexose transporter (g6695), a periplasmic β -glucosidase (g7443), and an intracellular β -glucosidase (g4171) (Fig. 2G). These are orthologs of *N. crassa* genes previously reported to be regulated by CLR1 during growth on cellulose (39). The decrease in the expression of these CWDEs did not correlate with changes in the gene expression of the carbon catabolite repressor *CRE1* (g6882) (fig. S5) (47). We detected a lower amount of residual cellulose in roots infected with WT compared to those infected with Δ *clr1* (Fig. 2H), in line with the results of growth on cellulose (Fig. 1, C and D, and fig. S3). Together, our data reveal that CLR1 is required by *Fo* for efficient degradation of cellulose during root colonization but dispensable for reaching the plant vasculature.

Arabidopsis defense response is delayed upon Δ *clr1-1* infection compared to WT

The reduction in cellulase activity observed in Δ *clr1-1* might reduce the amount and/or nature of the CW-derived DAMPs generated by this mutant compared to WTs. Therefore, the increased virulence

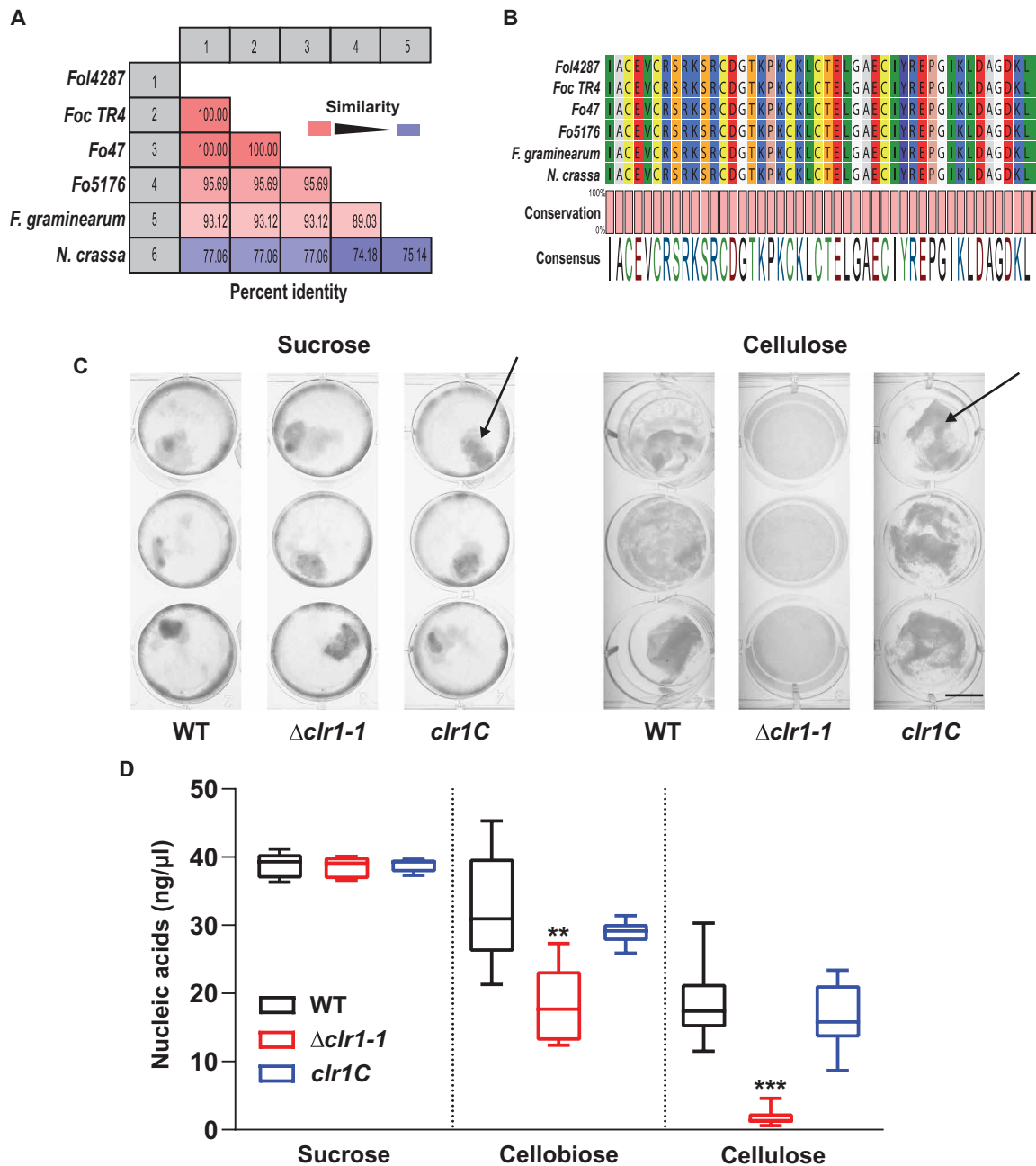


Fig. 1. Cellulose degradation is regulated by CLR1 in Fo (Fo5176). (A) Pairwise comparison of potential protein orthologs of *N. crassa* CLR1 from four *Fo* species complexes and *F. graminearum*, identified by BLAST analysis. The percent of protein identity is indicated. (B) Sequence alignment of the DNA binding domains of the CLR1 proteins confirmed as *N. crassa* orthologs in (A). The conservation grade is shown. Note the high conservation of the Zn(2)-C6 fungal-type domain, ACEVCRSRKSRCDGTPKPKCKLCTELGAECLYREPGKLDAGDKLI, confirmed as a DNA binding domain in *N. crassa*. (C) Representative picture of wild-type (WT), $\Delta clr1-1$, and *clr1C* growth on sucrose (left) or cellulose (right). The arrow indicates the presence of mycelia. Scale bar, 1 cm. (D) Growth of WT, $\Delta clr1-1$, and *clr1C* on different carbon sources measured as nucleic acid concentration (ng/μl). The strains were growing on 0.5% sucrose or 0.5% cellobiose for 3 days, or on 0.5% cellulose for 7 days. The box plots are shown: Centerlines show the medians; box limits indicate the 25th and 75th percentiles; whiskers extend to the minimum and maximum, $N \geq 5$. Asterisk indicated differences relative to WT. Welch's unpaired t test; *** $P < 0.001$, ** $P < 0.01$.

of the cellulase-deficient $\Delta clr1-1$ mutant might be a consequence of an impaired activation of plant immune responses. To address this hypothesis, we measured the expression of three genes previously reported to be activated in Arabidopsis roots infected by Fo5176: *At1g51890*, *WRKY45*, and *WRKY53* (33, 48). At 2 and 3 dpt, the expression of the three defense genes was lower in plants infected

with $\Delta clr1-1$ than WT (Fig. 3A). These differences progressively disappeared with the increased vascular colonization. At 7 dpt, when the xylem was abundantly occupied by $\Delta clr1-1$, the plant defense gene expression was higher than in roots infected with WT (Fig. 3A). These findings suggested that the higher number of vascular penetrations observed upon $\Delta clr1-1$ infection (Fig. 2A) might be a

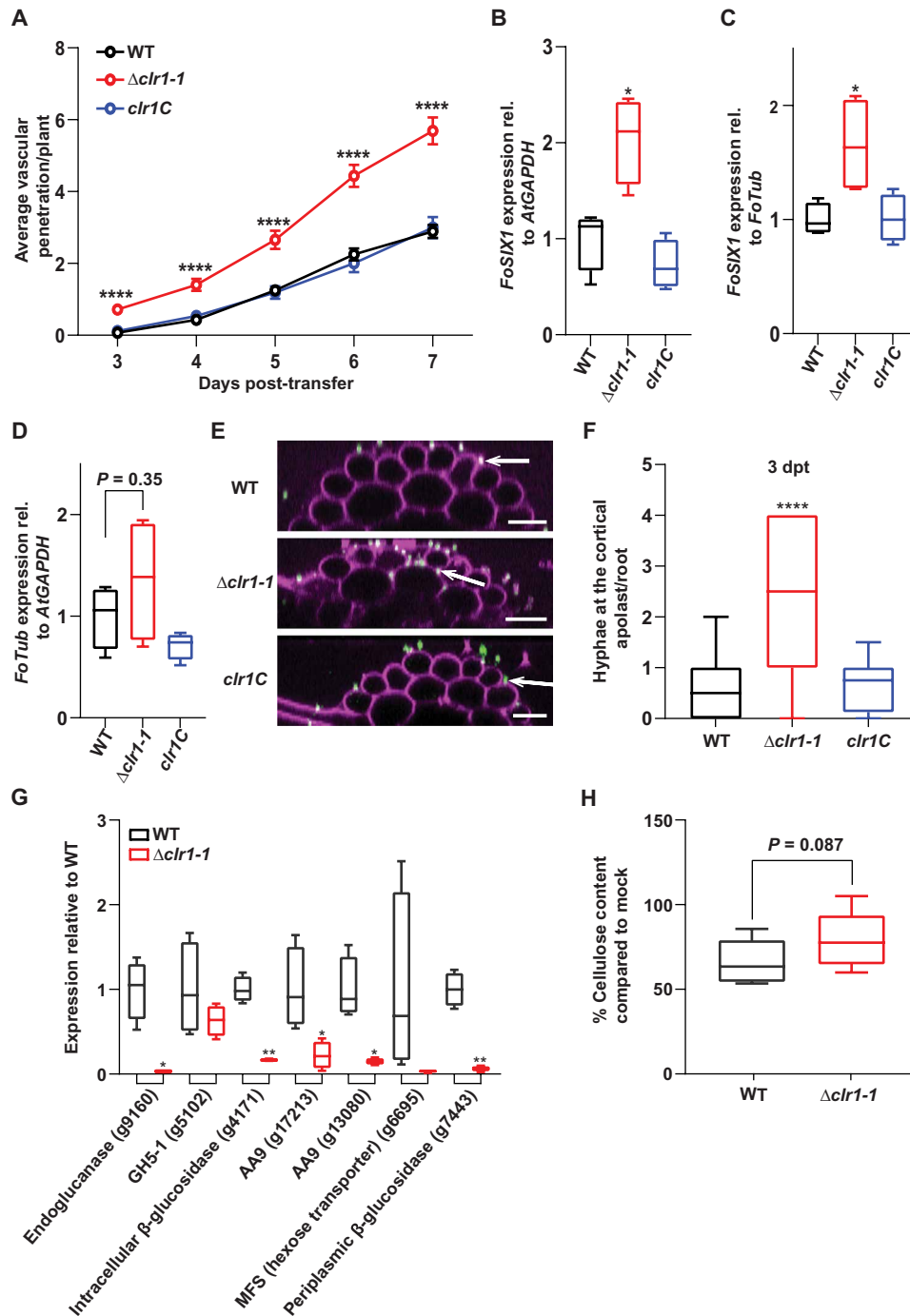


Fig. 2. The lack of CLR1 increases *Fo* pathogenicity. (A) Cumulative Arabidopsis root vascular penetration by *Fo* at different dpt to WT, $\Delta clr1-1$, or *clr1C* microconidia-containing plates. Means \pm SEM; $N \geq 26$ plants from one representative experiment. The experiment was performed three times with similar results. Repeated-measures (RM) two-way analysis of variance (ANOVA) on vascular penetration rate: $P < 0.0001$ (fungal genotype), $P < 0.0001$ (time), and $P < 0.0001$ (fungal genotype \times time). Tukey's multiple comparison test, **** $P < 0.0001$ with respect to WT at any dpt. (B and C) *FoSIX1* expression relative to *AtGAPDH* or *FoTub*, respectively, in infected Arabidopsis roots at 7 dpt as in (A). Box plots: Centerlines show the medians; box limits indicate the 25th and 75th percentiles; whiskers extend to the minimum and maximum. $N = 4$ biological replicates; Welch's unpaired *t* test; * $P < 0.05$. (D) Fungal biomass calculated as *FoTub* expression relative to *AtGAPDH*. Box plots, as above. $N = 4$ biological replicates. (E) Representative confocal image of WT, $\Delta clr1-1$, or *clr1C* hyphae (green, arrows) colonization of Arabidopsis roots (CW, magenta). Scale bars, 20 μ m. (F) Number of WT, $\Delta clr1-1$, or *clr1C* hyphae able to reach the cortical apoplast as shown in (E) per root. Box plots, as above; $N \geq 16$ roots. Welch's unpaired *t* test; **** $P < 0.0001$. (G) Expression of genes relative to *FoTub* in WT and $\Delta clr1-1$ at 7 dpt infected roots. The box plots are shown as described above, $N = 4$ biological replicates. For each gene, the data were normalized to WT; Welch's unpaired *t* test; * $P < 0.05$ and ** $P < 0.01$. (H) Cellulose content in WT- and $\Delta clr1-1$ -infected roots at 7 dpt represented as % of cellulose measured in 7-dpt mock roots. The box plots are shown as described above. $N = 8$ biological replicates. Welch's unpaired *t* test; *P* value is indicated.

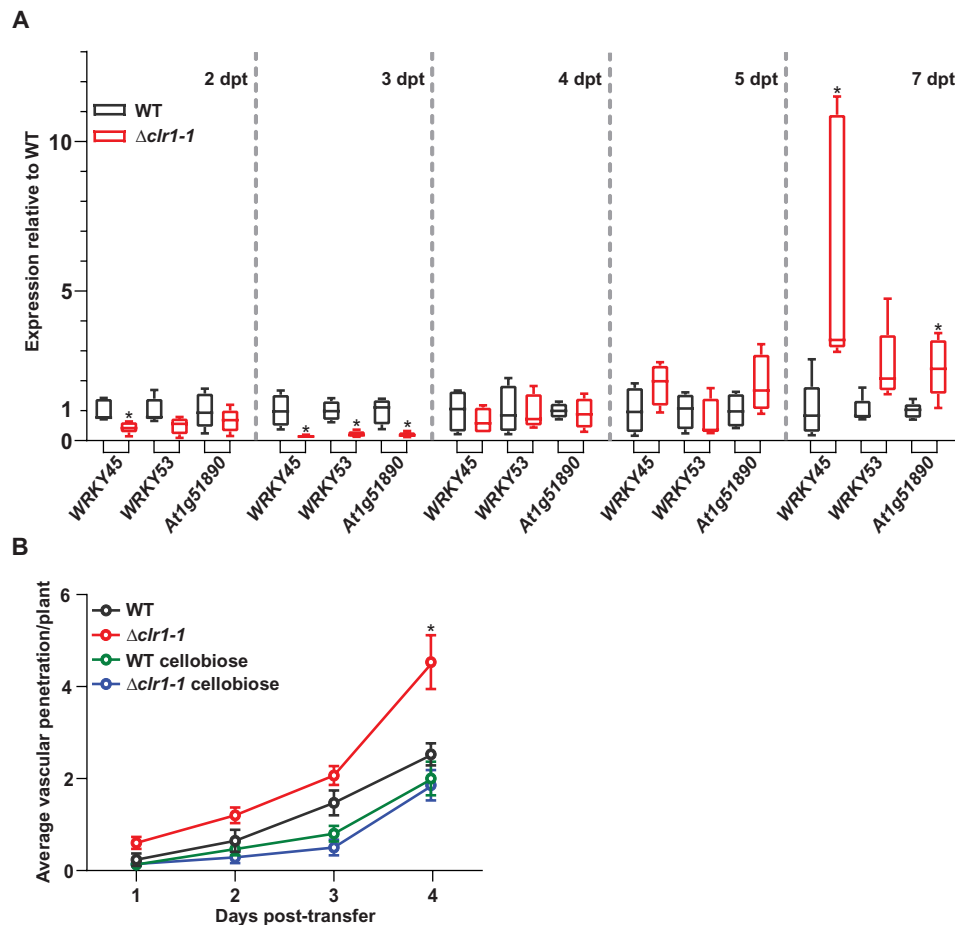


Fig. 3. The plant perceives later $\Delta clr1-1$ than WT. (A) Expression of *WRKY45*, *WRKY53*, and *At1g51890* relative to *AtGAPDH* in Arabidopsis roots at 2, 3, 4, 5, or 7 dpt to plates with WT or $\Delta clr1-1$ microconidia. The box plots are shown: Centerlines show the medians; box limits indicate the 25th and 75th percentiles; whiskers extend to the minimum and maximum; $N \geq 4$ biological replicates. For each gene, the data were normalized to WT and the statistical differences are indicated by asterisks; Welch's unpaired *t* test; $*P < 0.05$. (B) Cumulative Arabidopsis root vascular penetration by *Fo* at different dpt to WT or $\Delta clr1-1$, hyphae-containing plates. Half of the plants were pretreated with cellobiose for 25 min before being exposed to the fungus. Values are means \pm SEM, $N \geq 14$ from one representative experiment. The experiment was repeated three times with similar results. RM two-way ANOVA on vascular penetration rate: $P < 0.0001$ (fungal genotype and treatment), $P < 0.0001$ (time), and $P < 0.0001$ (fungal genotype \times time). Asterisk indicates a statistical difference with respect to WT at 4 dpt. Tukey's multiple comparisons test; $*P < 0.05$.

consequence of delayed activation of defense-related genes during the early stages of the interaction.

We next tested whether external addition of CW-derived DAMPs could reduce the virulence of $\Delta clr1-1$ to WT levels. We used cellobiose, a cellulose degradation product confirmed to induce plant defense (27), to prime the root immune system. As *Fo* can grow on cellobiose, exposing cellobiose-treated plants to fungal spores will significantly reduce the DAMP effect of this molecule in the latest days of our plate infection assay. Thus, we pretreated plants for 25 min with this cellobiose before transferring them to plates containing 3-day-old WT or $\Delta clr1-1$ mycelium. We confirmed that cellobiose-induced root defense priming returned the plant susceptibility of $\Delta clr1-1$ to WT levels (Fig. 3B).

Different amounts of CW degradation products accumulate upon $\Delta clr1-1$ infection

The reduced cellulose degradation and the concomitant absence or decrease of cellobiose in the apoplast during $\Delta clr1-1$ infection might explain the delay in perception of this mutant by the root and its

increased virulence. To test this idea, we measured the oligosaccharides derived from plant CW degradation by *Fo5176* using high-performance size exclusion chromatography by tandem mass spectrometry (HP-SEC-MS/MS) (49). By using different commercial standards representing the different hexoses and saturated OGs, we found that sucrose and another disaccharide were the main sugars present in mock-treated roots (Fig. 4A). In both WT- and $\Delta clr1-1$ -infected roots, we identified cellodextrins of up to six glucoses in length, being the cellobiose the most abundant one, at least 10 times more than the longer cellodextrins, and the only one whose relative amounts vary at different dpt (Fig. 4, B and C, and fig. S6B). Cellobiose was highly present in *Fo5176*-infected but not mock-treated roots, supporting its predicted role as DAMP (Fig. 4B). Our results showed a shift in the dihexose profiles from sucrose- to cellobiose-enriched at 2 and 3 dpt, respectively (Fig. 4B). From 3 dpt on the amount of dihexoses in the roots, mainly cellobiose was higher during infection with $\Delta clr1-1$ compared with WT (Fig. 4, B and C, and fig. S6). These results indicate that the impaired capacity of the plant to detect $\Delta clr1-1$ cannot be explained by a reduced release of

cellobiose by the mutant. We identified cellobiose-producing enzymes in the $\Delta clr1-1$ secretome, i.e., cellulases and xyloglucanases (Table 1). Therefore, we asked whether the higher levels of cellobiose detected in $\Delta clr1-1$ -infected roots were due to a misregulation of cellobiose transporters in the mutant. We identified in *N. crassa* (8): *CDT1* (g12318) and *CDT2* (g14945). *CDT2* was significantly down-regulated in the mutant, while *CDT1* expression remained as in WT fungus (Fig. 4F).

Then, we studied the OGs produced by Fo5176 and identified acetylated OGs as a main product of plant CW degradation by both $\Delta clr1-1$ and WT (Fig. 4, B, D, and E, and fig. S6C). Moreover, less OGs were detected during $\Delta clr1-1$ infection compared to WT-infected roots, especially at 3 and 4 dpt (Fig. 4, B, D, and E, and fig. S6). This difference was statistically significant for GalA₂ox and GalA₄Ac (Fig. 4, D and E). The decreased accumulation of OGs during the early stages of plant infection is in line with the compromised perception of $\Delta clr1-1$ by the plant. We detected significant differences in the amount of plant CW degradation products in WT- and $\Delta clr1-1$ -infected roots that might act as DAMPs. Therefore, we next tested whether WT-generated DAMPs can restore plant susceptibility to $\Delta clr1-1$ by performing plate infection assays using the same number of microconidia concentration of $\Delta clr1-1$, WT, or both (50% WT + 50% $\Delta clr1-1$). We expected to see a decrease in $\Delta clr1-1$ virulence proportional to the concentration of WT spores in the mixed treatment if DAMP accumulation is the main reason for the differential plant susceptibility to $\Delta clr1-1$ and WT. By contrast, we found that the 50% mixed infection displayed the same pathogenicity as $\Delta clr1-1$ alone (fig. S7A), observing a decrease in xylem penetration only when 90% of the spores were WT (fig. S7B). Our data indicate that although $\Delta clr1-1$ infection generates different amounts of CW degradation products than WT, they alone do not explain $\Delta clr1-1$ higher pathogenicity.

$\Delta clr1-1$ secretes more virulence factors than WT during root colonization

Pathogenicity relies on the ability of microorganisms to evade the MAMP- and DAMP-induced host defenses using secreted and cell surface localized virulence factors (50). We performed proteomic analysis of the secretomes of WT and $\Delta clr1-1$ during plant infection to determine whether differences in their profile of secreted virulence factors could explain the higher virulence of $\Delta clr1-1$. Seedlings growing in hydroponics were inoculated with either WT or $\Delta clr1-1$ microconidia. Three hundred sixty-two fungal proteins were identified, 75% with predicted secretory signal peptides. Of these, more than 30% belong to groups considered as virulence factors in other plant pathogens such as *Fusarium graminearum* (50), including glycosyl hydrolases (24.3%), peptidases (10.8%), redox-related proteins (8.6%), and pectin and pectate lyases (4.1%) (Fig. 5A).

As expected, we found a significant reduction in the abundance of proteins required for cellulose degradation in the $\Delta clr1-1$ secretome (Fig. 5B and Table 1), including GH5 (g17181), GH6 (g15944), and GH7 (g873), which are predicted to exhibit cellulolytic activity (51), as well as AA9s (g15991) and (g13080) that make crystalline cellulose accessible to cellulases (9). These data confirm the down-regulation of cellulase-related genes observed in $\Delta clr1-1$ and explain its reduced capacity to degrade cellulose (Figs. 1, C and D, and 2, G and H, and fig. S3).

In contrast, we found an increased presence of other virulence factors in the secretome of $\Delta clr1-1$ compared to that of WT (Fig. 5B

and Table 1). $\Delta clr1-1$ releases increased amounts of a protein (g2038) annotated as a cutinase, which was reported to be essential for virulence of necrotrophic fungal pathogens (52). In addition, we found an increase in pectin and pectate lyases in the $\Delta clr1-1$ secretome (53–55). Similarly, a set of eight peptidases previously described as critical virulence factors (56) were more abundant in the $\Delta clr1-1$ secretome. These included four subtilases and fungalysin, among others (Table 1). The subtilases are able to degrade plant proteins with antifungal activity, such as β 1-3 glucanases (57). The fungalysin proteins compromise host defense by cleaving class IV plant chitinases, preventing the release of the MAMP chitin and, as such, have been reported to be necessary for the virulence of several plant pathogenic filamentous ascomycetes, including *Ustilago maydis*, *Fo f. sp. lycopersici* (Fol), *Fusarium verticillioides*, and *Colletotrichum graminicola* (58–61). Last, we noticed an enrichment in a chitin deacetylase, whose orthologs impede chitin-triggered immunity in cotton by converting chitin oligomers into ligand-inactive molecules like chitosan (62). Our data indicate that $\Delta clr1-1$ reduces the plant detection of its chitin, which could explain its increased virulence and the reduced host defense (Figs. 2A and 3A). To test this possibility, we performed a chitin-dependent defense priming assay as previously done for cellobiose (Fig. 3B). When roots were pretreated with chitin, the plant susceptibility to $\Delta clr1-1$ was indistinguishable from that observed against WT Fo5176 (Fig. 5C).

We next investigated the role of sugar availability on the up-regulation of the virulence factors enriched in the $\Delta clr1-1$ secretome. We measured the expression of six of these genes (g16048, g2038, g7764, g1489, g15798, and g11385) in WT and $\Delta clr1-1$ grown on sucrose or cellulose or in infected roots at 3 dpt. We observed a general increase in the expression of all genes in $\Delta clr1-1$ compared to WT when growing on cellulose and in planta (Fig. 5, E and F), while no differences were observed between the strains grown on sucrose (Fig. 5D). These results suggest that $\Delta clr1-1$ increases both the expression and secretion of various virulence factors to compensate for its decreased ability to use cellulose as a primary carbon source.

CLR1 is essential to complete Fo life cycle

Our data indicated that CLR1 is not required for Fo5176 to reach and enter the xylem and question the biological relevance of this transcription factor in Fo growth in planta. To shed light on this, we studied the temporal transcriptional regulation of *CLR1* in infected roots. *CLR1* expression increased significantly from 4 dpt on, especially after 5 dpt (Fig. 6A), growing exponentially until 7 dpt, when Fo5176 had already proliferated in the vasculature. This suggests that cellulases might play a critical role in the final infection stages. We therefore explored CLR1 function during the final phase of the host-fungus interaction, saprophytic growth, which is an important part of the Fo life cycle. When Fo5176 was grown for 4 days on dead or living plants, we observed three times more expression of *CLR1* under saprophytic than under hemibiotrophic growth conditions (Fig. 6B). The last step of a fungal life cycle is the production of spores. Therefore, we tested the impact of CLR1 on microconidia production on dead seedlings. Our data showed that WT and *clr1C* produced five times more microconidia than $\Delta clr1-1$ (Fig. 6C). Together, these findings indicate that CLR1 is essential for saprophytic growth and spore production of Fo on dead plant tissue.

Table 1. Fo5176 secretome identified proteins. Proteins identified in the secretomes of WT- and Δ clr1-1-infected roots at 3 dpt. A moderate t test P value was used for statistical analysis. (N = 4 biological replicates). For the proteins without InterPro (IPR) description, no homologs were found in the database to assign a putative activity.

Gene ID	IPR description	Δ clr1-1	WT	Log ₂ FC	P	Adjusted P
g15944	Glycoside hydrolase, family 6, conserved site, 1, 4-beta cellobiohydrolase, cellulose-binding domain, fungal, 1, 4-beta cellobiohydrolase superfamily, cellulose-binding domain superfamily	1.10	6.26	5.16	4.686×10^{-6}	0.001186
g873	Cellulose-binding domain, fungal, glycoside hydrolase, family 7, concanavalin A-like lectin/glucanase domain superfamily, glycoside hydrolase family 7, catalytic domain superfamily, cellulose-binding domain superfamily	-1.06	7.35	8.41	9.181×10^{-6}	0.001186
g17181	Glycoside hydrolase, family 5, cellulose-binding domain, fungal, cellulose-binding domain superfamily, glycoside hydrolase superfamily	0.44	5.28	4.84	9.831×10^{-6}	0.001186
g15991	Glycoside hydrolase, family 61	1.09	5.46	4.37	3.777×10^{-5}	0.003418
g13080	Glycoside hydrolase, family 61	-2.93	2.19	5.12	7.944×10^{-5}	0.005752
g2038	Alpha/beta hydrolase fold, cutinase, monofunctional, cutinase/acylxylan esterase	4.10	0.18	-3.91	0.0001006	0.006069
g5928	Copper amine oxidase, N2-terminal, domain of unknown function DUF1965, copper amine oxidase, copper amine oxidase, N-terminal, copper amine oxidase, catalytic domain superfamily, copper amine oxidase, catalytic domain	2.73	-2.56	-5.29	0.0001452	0.007510
g7764	Peptidase S8/S53 domain superfamily, peptidase S8, subtilisin-related, peptidase S8, subtilisin, His-active site, peptidase S8, subtilisin, Asp-active site, peptidase S8, subtilisin, Ser-active site, peptidase S8 propeptide/proteinase inhibitor I9 superfamily, peptidase S8/S53 domain, proteinase K-like catalytic domain	0.34	-2.07	-2.41	0.001898	0.085018
g3515	Cyclophilin-type peptidyl-prolyl cis-trans isomerase domain, cyclophilin-like domain superfamily, cyclophilin-type peptidyl-prolyl cis-trans isomerase, conserved site	-1.56	0.88	2.44	0.0021137	0.085018
g4964	FAD/NAD(P)-binding domain superfamily, glucose-methanol-choline oxidoreductase, N-terminal, glucose-methanol-choline oxidoreductase, glucose-methanol-choline oxidoreductase, C-terminal	4.68	3.05	-1.63	0.0027534	0.099672
g4855	WD40/YVTN repeat-like-containing domain superfamily	4.60	6.17	1.57	0.0032941	0.108405
g12830	GDSL lipase/esterase, SGNH hydrolase superfamily	-0.54	1.50	2.05	0.0040273	0.116412
g12342	Glucose-methanol-choline oxidoreductase, C-terminal, glucose-methanol-choline oxidoreductase, N-terminal, FAD/NAD(P)-binding domain superfamily, glucose-methanol-choline oxidoreductase	1.37	-1.01	-2.37	0.0041805	0.116412
g17742	Esterase, PHB depolymerase, cellulose-binding domain, fungal, alpha/beta hydrolase fold	0.74	2.35	1.61	0.0046421	0.120031
g3198	Glycoside hydrolase, family 29, glycoside hydrolase superfamily, alpha-L-fucosidase, metazoan-type	-2.16	0.73	2.89	0.0054141	0.128718
g7360	Glucose-methanol-choline oxidoreductase, N-terminal, glucose-methanol-choline oxidoreductase, C-terminal, cellobiose dehydrogenase, cytochrome domain, FAD/NAD(P)-binding domain superfamily, CHD, cytochrome domain superfamily	0.02	-2.14	-2.16	0.0057784	0.128718
g7411	Glucose-methanol-choline oxidoreductase, N-terminal, glucose-methanol-choline oxidoreductase, C-terminal, cellobiose dehydrogenase, cytochrome domain, FAD/NAD(P)-binding domain superfamily, CHD, cytochrome domain superfamily	-1.99	-4.70	-2.71	0.0061859	0.128718
g10128	FAD/NAD(P)-binding domain superfamily	-4.28	-1.68	2.61	0.0064004	0.128718
g11385	Glycoside hydrolase/deacetylase, beta/alpha barrel, NodB homology domain	1.70	-0.58	-2.28	0.0075396	0.136344
g15798	Peptidase M36, fungalsin, FTP domain, peptidase M4/M1, CTD superfamily	7.12	5.64	-1.48	0.0076433	0.136344
g5082	Cellulose-binding domain superfamily, cellulose-binding domain, fungal, glycosyl hydrolases family 10, active site, glycoside hydrolase superfamily, glycoside hydrolase family 10 domain	3.02	6.09	3.08	0.0102736	0.177098
g16180	Pectin lyase fold/virulence factor, pectinesterase, catalytic, pectin lyase fold, pectinesterase, Asp active site	-1.93	-3.69	-1.76	0.0120824	0.197791
g10757	Pectin lyase fold/virulence factor, pectinesterase, catalytic, pectin lyase fold, pectinesterase, Asp active site	-1.71	-0.05	1.66	0.0125668	0.197791
g2525	LysM domain, LysM domain superfamily	-4.45	-1.55	2.90	0.0145568	0.219565
g11976	Alpha/beta hydrolase fold, esterase, PHB depolymerase	1.72	4.06	2.34	0.0173639	0.251429
g12120	Glycosyl hydrolase, five-bladed beta-propeller domain superfamily, glycoside hydrolase, family 43, concanavalin A-like lectin/glucanase domain superfamily, beta-xylosidase, C-terminal concanavalin A-like domain	1.43	2.96	1.53	0.0213936	0.278408
g16048	Pectate lyase P1/H/P1/H-like, pectin lyase fold, pectin lyase fold/virulence factor	-2.25	-4.98	-2.73	0.0228618	0.278408
g1489	Peptidase S8, subtilisin, Ser-active site, peptidase S8, subtilisin, Asp-active site, peptidase S8/S53 domain superfamily, peptidase S8, subtilisin-related, proteinase K-like catalytic domain, peptidase S8, subtilisin, His-active site, peptidase S8/S53 domain, peptidase S8 propeptide/proteinase inhibitor I9, peptidase S8 propeptide/proteinase inhibitor I9 superfamily	3.40	1.04	-2.36	0.0229486	0.278408

continued on next page

Gene ID	IPR description	$\Delta cfr1-1$	WT	Log ₂ FC	P	Adjusted P
g9438	FAD-linked oxidase, N-terminal, FAD-binding domain, PCMH-type, FAD-binding, type PCMH-like superfamily	3.37	1.72	-1.65	0.0230994	0.278408
g16997	Pectin lyase fold/virulence factor, pectin lyase fold, PL-6 family, right-handed beta helix domain	1.07	-0.02	-1.09	0.0238461	0.278408
g15934	GD5L lipase/esterase, SGNH hydrolase superfamily	-0.80	2.12	2.92	0.0242533	0.278408
g15471	Glycoside hydrolase, family 32, glycosyl hydrolase, five-bladed beta-propeller domain superfamily, glycosyl hydrolase family 32, C-terminal, concanavalin A-like lectin/glycanase domain superfamily, glycosyl hydrolase family 32, N-terminal	-1.95	0.49	2.45	0.0246107	0.278408
g15630	Proteinase K-like catalytic domain, peptidase S8, subtilisin, Asp-active site, peptidase S8/S53 domain superfamily, peptidase S8 propeptide/proteinase inhibitor I9 superfamily, peptidase S8, subtilisin, Ser-active site, peptidase S8/S53 domain, peptidase S8, subtilisin-related	1.90	0.56	-1.34	0.0269427	0.288834
g1832	Proteinase K-like catalytic domain, peptidase S8, subtilisin, Asp-active site, peptidase S8/S53 domain, peptidase S8 propeptide/proteinase inhibitor I9 superfamily, peptidase S8, subtilisin, His-active site, peptidase S8/S53 domain superfamily, peptidase S8, subtilisin-related, peptidase S8 propeptide/proteinase inhibitor I9, peptidase S8, subtilisin, Ser-active site	3.79	2.44	-1.35	0.0275055	0.288834
g9050		1.42	2.54	1.12	0.028448	0.288834
g6456	Heat shock protein 70 family, heat shock protein 70 kDa, C-terminal domain superfamily, heat shock protein 70 kDa, peptidase-binding domain superfamily, ATPase, nucleotide binding domain, heat shock protein 70, conserved site, endoplasmic reticulum chaperone BIP, nucleotide-binding domain	-4.46	-2.24	2.22	0.0287238	0.288834
g6198	Glucanoyltransferase, glycoside hydrolase superfamily	-1.44	0.04	1.49	0.0303203	0.296647
g5964	Peptidase S10, serine carboxypeptidase, alpha/beta hydrolase fold, serine carboxypeptidase, serine active site	-0.11	-1.97	-1.86	0.0338176	0.321392
g17041	Necrosis-inducing protein	-1.80	-0.28	1.52	0.0351755	0.321392
g9531	S1/P1 nuclease, phospholipase C/P1 nuclease domain superfamily	-0.70	-2.89	-2.20	0.035513	0.321392
g12993	EMP46/EMP47, N-terminal lectin domain, concanavalin A-like lectin/glycanase domain superfamily, legume-like lectin	-3.44	-1.71	1.72	0.0384319	0.335491
g15873	Glycoside hydrolase, family 3, N-terminal domain superfamily, glycoside hydrolase, family 3, N-terminal, fibronectin type III-like domain, glycoside hydrolase superfamily, glycoside hydrolase family 3 C-terminal domain, glycoside hydrolase family 3 C-terminal domain superfamily, glycoside hydrolase, family 3, active site, immunoglobulin-like fold	2.15	0.80	-1.35	0.0389244	0.335491
g15992	Tuberculosis-necrotizing toxin	-2.78	-1.69	1.09	0.0445783	0.338676
g8603	Glycosyl hydrolase, five-bladed beta-propeller domain superfamily, glycoside hydrolase, family 43	0.00	-1.35	-1.35	0.0451032	0.338676
g6954	Rho protein GDP-dissociation inhibitor, Rho GDP-dissociation inhibitor domain superfamily, immunoglobulin E-set	-4.17	-2.08	2.09	0.0453064	0.338676
g4912	Serine proteases, trypsin family, histidine active site, peptidase S1A, chymotrypsin family, peptidase S1, PA clan, chymotrypsin-like fold, serine proteases, trypsin domain, peptidase S1, PA clan, serine proteases, trypsin family, serine active site	7.44	6.23	-1.21	0.0453677	0.338676
g8786	GLEYA adhesin domain, PA14/GLEYA domain	1.44	0.34	-1.10	0.0456485	0.338676
g17064	Endonuclease/exonuclease/phosphatase superfamily	1.41	-0.16	-1.56	0.0457507	0.338676
g704	Ran GTPase, small GTP-binding protein domain, P-loop containing nucleoside triphosphate hydrolase, small GTPase	-1.76	-0.41	1.35	0.0463791	0.338676
g1768	Pepsin-like domain, aspartic peptidase A1 family, aspartic peptidase, active site, aspartic peptidase domain superfamily, peptidase family A1 domain	1.24	-0.82	-2.06	0.0467784	0.338676
g7485		1.42	2.40	0.97	0.0492285	0.341361
g10337		0.43	2.07	1.64	0.0494591	0.341361
g951	Glycoside hydrolase superfamily	-2.99	-0.63	2.36	0.0502738	0.341361
g837	YigF/YER057_cUK1 14 family, RidA family, RidA, conserved site, RutC-like superfamily	-4.66	-3.15	1.51	0.0509212	0.341361
g15627	Necrosis-inducing protein	0.53	-0.66	-1.19	0.0548193	0.359712
g17579	isochorismatase-like superfamily, isochorismatase-like	0.78	2.10	1.32	0.0562913	0.359712
g7398	Short-chain dehydrogenase/reductase SDR, NAD(P)-binding domain superfamily	-1.14	-3.42	-2.28	0.0566397	0.359712
g8556	Tyrosinase copper-binding domain, uncharacterized domain, di-copper center	-0.13	-3.21	-3.08	0.0578008	0.360757
g6750	Glycoside hydrolase, family 61	1.57	2.52	0.95	0.0609251	0.373812

continued on next page

Gene ID	IPR description	Δ cdt1-1	WT	Log ₂ FC	P	Adjusted P
g12184	Peroxiredoxin, C-terminal, peroxiredoxin, AhpC-type, thioredoxin-like superfamily, thioredoxin domain, alkyl hydroperoxide reductase subunit C/thiol-specific antioxidant	-2.68	-1.22	1.46	0.0640908	0.386681
g14800	Glycoside hydrolase, family 61	0.15	-0.95	-1.10	0.0675119	0.399896
g9034	Thioredoxin-like superfamily, domain of unknown function DUF953, thioredoxin-like	-1.65	-2.82	-1.18	0.0684906	0.399896
g1456	Cyclophilin-type peptidyl-prolyl cis-trans isomerase, conserved site, cyclophilin-type peptidyl-prolyl cis-trans isomerase domain, cyclophilin-like domain superfamily, cyclophilin-type peptidyl-prolyl cis-trans isomerase	-3.28	-1.20	2.07	0.0750687	0.429309
g944	Inorganic pyrophosphatase superfamily, inorganic pyrophosphatase	-4.66	-2.47	2.19	0.076033	0.429309
g6384	Glutathione reductase, eukaryote/bacteria, FAD/NAD(P)-binding domain superfamily, FAD/NAD-linked reductase, dimerization domain superfamily, pyridine nucleotide-disulfide oxidoreductase, class I, pyridine nucleotide-disulfide oxidoreductase, dimerization domain, FAD/NAD(P)-binding domain, pyridine nucleotide-disulfide oxidoreductase, class I, active site	-3.20	-0.41	2.79	0.0770859	0.429309
g8150	Alpha/beta hydrolase fold, alpha/beta hydrolase fold-1	-3.44	-2.09	1.35	0.0796829	0.437049
g14988		-2.38	-4.11	-1.73	0.0857754	0.463443
g14301	Inositol oxygenase	-3.04	-0.87	2.17	0.0880556	0.468767
g8422	Heat shock protein 70 kDa, C-terminal domain superfamily, ATPase, nucleotide binding domain, heat shock protein 70, conserved site, heat shock protein 70 kDa, peptide-binding domain superfamily, heat shock protein 70 family	-4.17	-1.82	2.36	0.0895721	0.469929
g5368	Alpha/beta hydrolase fold, cutinase/acetylcholin esterase, cutinase, monofunctional	2.29	0.83	-1.46	0.0919153	0.475333
g11902	RlpA-like domain superfamily, expansin, cellulose-binding-like domain superfamily, expansin/pollen allergen, DPB5 domain	-0.02	-1.64	-1.63	0.0939064	0.478790
g13461		7.39	6.06	-1.33	0.0976655	0.491041
g2604		-5.15	0.92	6.08	0.1001677	0.496722
g1758	Alpha carboxylic anhydride domain, carbonic anhydrase, alpha class, alpha carboxylic anhydride domain superfamily, carbonic anhydrase, prokaryotic-like	-0.32	0.47	0.79	0.1045865	0.511626
g13593		2.00	3.47	1.47	0.1117582	0.537084
g3337	Glycosyl hydrolase, five-bladed beta-propeller domain superfamily, glycoside hydrolase, family 62, arabinosidase	3.82	5.32	1.50	0.1159258	0.537084
g4548	ACP-like superfamily, phosphopantetheine binding ACP domain, trimeric LpxA-like superfamily, AMP-dependent synthetase-like superfamily, polyketide synthase, phosphopantetheine-binding domain, AMP-dependent synthetase/ligase	-1.20	-2.32	-1.12	0.117796	0.537084
g11299	Immunoglobulin-like fold, glycoside hydrolase family 3 C-terminal domain superfamily, glycoside hydrolase, family 3, N-terminal, fibronectin type III-like domain, glycoside hydrolase family 3 C-terminal domain, glycoside hydrolase, family 3, N-terminal domain superfamily, glycoside hydrolase superfamily	2.91	2.08	-0.83	0.1183346	0.537084
g15930	Beta-xylosidase, C-terminal concanavalin A-like domain, glycoside hydrolase, family 43, concanavalin A-like lectin/glucanase domain superfamily, glycosyl hydrolase, five-bladed beta-propeller domain superfamily	3.63	4.36	0.72	0.1183713	0.537084
g10243		0.38	-0.37	-0.76	0.11882	0.537084
g4447	Peptidase M28, PA domain, peptidase M28, SGAP-like	-0.31	0.93	1.24	0.1218241	0.537084
g17329	Major facilitator superfamily, alpha/beta hydrolase fold, peptidase S9, prolyl oligopeptidase, catalytic domain, MFS transporter superfamily	-0.91	-0.03	0.88	0.1221296	0.537084
g9446	Oxidoreductase, C-terminal, oxidoreductase, N-terminal, NAD(P)-binding domain superfamily	-2.45	-1.51	0.94	0.1238965	0.537084
g15661	Uncharacterized domain, di-copper center, tyrosinase copper-binding domain	-1.33	-2.36	-1.03	0.1246272	0.537084
g8037	Glycoside hydrolase superfamily, glycoside hydrolase family 17	2.58	0.02	-2.57	0.1313975	0.555750
g5019	Alpha-L-fucosidase, metazoan-type, glycoside hydrolase superfamily, glycosyl hydrolase, all-beta, alpha-L-fucosidase, C-terminal, glycoside hydrolase, family 29	2.00	0.76	-1.24	0.1369409	0.555750
g1132	Uncharacterized protein family, glycosyl hydrolase catalytic domain, glycoside hydrolase superfamily	-0.01	1.11	1.12	0.1374093	0.555750
g15834	Chorismate mutase II, prokaryotic-type, chorismate mutase domain superfamily, chorismate mutase type II superfamily	-3.81	-5.14	-1.33	0.138957	0.555750
g13117	Peptidase S53, activation domain, peptidase S8/S53 domain superfamily, sedolisin domain, peptidase S8/S53 domain, peptidase S8, subtilisin, Ser-active site	0.58	-0.91	-1.50	0.1394611	0.555750
g16179	Pectin lyase fold, glycoside hydrolase, family 28, pectin lyase fold/virulence factor	-0.99	-2.33	-1.34	0.1401378	0.555750
g15705	Pectin lyase fold/virulence factor, pectin lyase fold	3.91	4.82	0.91	0.1411062	0.555750
g16885	Six-hairpin glycosidase superfamily, beta-L-arabinofuranosidase, GH127	-1.78	-3.59	-1.82	0.1412403	0.555750

continued on next page

Gene ID	IPR description	$\Delta cfr1-1$	WT	Log ₂ FC	P	Adjusted P
g7119	SUN family	-4.54	-2.81	1.73	0.1437161	0.559411
g14313	Transcription factor, GTP-binding domain, translation elongation factor EFTu-like, domain 2, P-loop containing nucleoside triphosphate hydrolase, GTP-binding protein 1, GTP binding protein 1-like, GTP-binding domain, translation elongation factor EFT1A/initiation factor IF2gamma, C-terminal, translation protein, beta barrel domain superfamily, translation elongation factor EFTu/EFT1A, C-terminal	-0.55	-1.47	-0.92	0.1466577	0.564788
g10908	Glycosyl hydrolase family 32, N-terminal, glycosyl hydrolase, five-bladed beta-propeller domain superfamily	4.65	5.29	0.65	0.1511474	0.575951
g16076	Glucose-methanol-choline oxidoreductase, N-terminal, glucose-methanol-choline oxidoreductase, C-terminal, FAD/NAD(P)-binding domain superfamily, glucose-methanol-choline oxidoreductase	3.83	3.07	-0.76	0.1557421	0.587278
g160	Leucine-rich repeat, leucine-rich repeat domain superfamily, leucine-rich repeat, typical subtype	-0.59	0.23	0.82	0.1578084	0.588934
g10104	Glycosyl hydrolase, five-bladed beta-propeller domain superfamily, concanavalin A-like lectin/glucanase domain superfamily, glycosyl hydrolase family 32, C-terminal, glycoside hydrolase, family 32, glycosyl hydrolase family 32, N-terminal	2.19	4.02	1.83	0.1655212	0.602413
g1461	Cutinase/acetylglucosaminidase, alpha/beta hydrolase fold	2.97	3.80	0.83	0.1675246	0.602413
g11425	Six-hairpin glycosidase superfamily, glycoside hydrolase, family 37, six-hairpin glycosidase-like superfamily, glycoside hydrolase, family 37, conserved site	-1.98	-3.47	-1.49	0.1683314	0.602413
g11287		1.42	0.45	-0.97	0.1690967	0.602413
g4077	Farnesyl pyrophosphatase synthase-like, polyprenyl synthetase, conserved site, isoprenoid synthase domain superfamily, polyprenyl synthetase	-5.35	-3.19	2.15	0.1697407	0.602413
g1642	Concanavalin A-like lectin/glucanase domain superfamily, glycoside hydrolase family 16	1.84	2.83	0.98	0.1727307	0.604016
g8629	Glycoside hydrolase, family 27, aldolase-type TIM barrel, alpha galactosidase, C-terminal beta sandwich domain, glycosyl hydrolase, all-beta, glycoside hydrolase superfamily, glycoside hydrolase family 27/36, conserved site	1.88	2.81	0.93	0.1735296	0.604016
g15670	Chitin-binding, type 1, conserved site, chitin-binding, type 1, glycosyl hydrolases family 18 (GH18) active site, endochitinase-like superfamily, glycoside hydrolase family 18, catalytic domain, chitinase II, glycoside hydrolase superfamily, chitinase insertion domain superfamily	-2.83	-4.74	-1.91	0.1812619	0.624922
g1682	SGNH hydrolase superfamily, rhamnogalacturonan acetyltransferase RhaGT-like, SGNH hydrolase-type esterase domain	1.58	0.80	-0.78	0.1860369	0.629416
g16522	DNA/RNA polymerase superfamily, reverse transcriptase domain, ribonuclease H superfamily, endonuclease/exonuclease/phosphatase superfamily, endonuclease/exonuclease/phosphatase, ribonuclease H domain	-5.77	-2.54	3.24	0.1860429	0.629416
g2432	Glycoside hydrolase, family 27, galactose-binding-like domain superfamily, glycosyl hydrolase, all-beta, aldolase-type TIM barrel, glycoside hydrolase superfamily, alpha galactosidase, C-terminal beta sandwich domain	0.56	-0.22	-0.78	0.1939755	0.644992
g4902		1.43	0.04	-1.39	0.1942103	0.644992
g10652	Allergen Asp f4	3.68	5.04	1.36	0.201376	0.662710
g14783	Glycoside hydrolase, family 43, galactose-binding-like domain superfamily, glycosyl hydrolase, five-bladed beta-propeller domain superfamily	3.55	2.64	-0.91	0.2057393	0.667896
g10105	Concanavalin A-like lectin/glucanase domain superfamily, glycoside hydrolase, family 32, glycosyl hydrolase family 32, N-terminal, glycosyl hydrolase, five-bladed beta-propeller domain superfamily, glycosyl hydrolase family 32, C-terminal	3.52	4.58	1.06	0.207311	0.667896
g8299	Galactose-binding-like domain superfamily, SGNH hydrolase superfamily, CICE2-like domain, SGNH hydrolase-type esterase domain, carbohydrate esterase 2, N-terminal	4.35	4.93	0.58	0.2084868	0.667896
g7394	Glycoside hydrolase, family 61	0.32	-0.49	-0.80	0.2144568	0.670561
g8868		-2.28	-3.36	-1.07	0.2183308	0.670561
g352	Peptidase S28, alpha/beta hydrolase fold	3.04	2.44	-0.60	0.2184503	0.670561
g10771	Expansin, cellulose-binding-like domain superfamily, RipA-like domain superfamily	4.22	3.44	-0.78	0.2191943	0.670561
g7502	Glycoside hydrolase superfamily, glycoside hydrolase, family 3, N-terminal, glycoside hydrolase family 3 C-terminal domain superfamily, glycoside hydrolase, family 3, N-terminal domain superfamily	3.75	3.07	-0.68	0.2200853	0.670561
g2577	Peptidase, metalloprotease, peptidase M12A, metalloprotease, catalytic domain superfamily	0.49	1.12	0.63	0.2212457	0.670561
g16090	Berberine/berberine-like, FAD-binding domain, PCMH-type, FAD-binding, type PCMH-like superfamily, FAD-linked oxidase, N-terminal	-1.37	-2.26	-0.89	0.2222854	0.670561
g7661	Glycoside hydrolase family 16, concanavalin A-like lectin/glucanase domain superfamily, glycoside hydrolase, family 16, CRH1, predicted	1.24	2.02	0.78	0.2260904	0.674745
g17217	Glycosyl hydrolase, family 13, catalytic domain, alpha-amylase-like, glycoside hydrolase superfamily	7.28	6.51	-0.78	0.2274004	0.674745

continued on next page

Gene ID	IPR description	$\Delta cfr1-1$	WT	Log ₂ FC	P	Adjusted P
g6054	SurE-like phosphatase/nucleotidase superfamily, survival protein SurE-like phosphatase/nucleotidase	3.14	2.39	-0.76	0.2311019	0.680154
g8752	Galactose mutarotase-like domain superfamily, glycoside hydrolase-type carbohydrate-binding, aldose 1-glucose-6-phosphate 1-epimerase	-0.33	-1.24	-0.91	0.2333957	0.681365
g10423	Aspartic peptidase domain superfamily, peptidase family A1 domain, aspartic peptidase A1 family, pepsin-like domain	-2.77	-1.70	1.08	0.2368871	0.686025
g4469	Cellulose/chitin-binding protein, N-terminal	1.54	0.88	-0.66	0.2393601	0.687685
g15672	LysM domain, LysM domain superfamily	-2.54	-1.37	1.17	0.2427509	0.691936
g6006	Glycoside hydrolase family 12, concanavalin A-like lectin/glucanase domain superfamily, glycoside hydrolase family 11/12	1.47	0.75	-0.73	0.249115	0.701318
g5159	Lactonase, 7-bladed beta propeller, WD40/YVTN repeat-like-containing domain superfamily, cytochrome cO1-nitrite reductase-like, haem d1 domain superfamily	1.31	2.09	0.77	0.2511583	0.701318
g9752	FAD-binding domain, PCMH-type, FAD-linked oxidase, N-terminal, FAD-binding, type PCMH-like superfamily, berberine/berberine-like	3.61	3.05	-0.56	0.2518544	0.701318
g9893		-3.35	-1.84	1.51	0.2553683	0.705674
g867	Superoxide dismutase, copper/zinc binding domain, superoxide dismutase (Cu/Zn)/superoxide dismutase-copper-chaperone, superoxide dismutase-like, copper/zinc binding domain superfamily	-0.65	-1.32	-0.67	0.2677532	0.709457
g15445	FAD-binding, type PCMH-like superfamily, FAD-linked oxidase, N-terminal, FAD-binding domain, PCMH-type	-0.79	-1.46	-0.67	0.2728442	0.709457
g637	Lumazine/riboflavin synthase superfamily, lumazine synthase, lumazine/riboflavin synthase	-2.70	-1.93	0.77	0.2734074	0.709457
g7298	Glycoside hydrolase family 16, concanavalin A-like lectin/glucanase domain superfamily	6.79	6.26	-0.53	0.2735358	0.709457
g7659	Pectate lyase, pectin lyase fold, pectin lyase fold/virulence factor	3.84	3.35	-0.49	0.2736414	0.709457
g457	Enolase, enolase, conserved site, enolase, C-terminal TIM barrel domain, enolase-like, N-terminal, enolase-like, C-terminal domain superfamily, enolase, N-terminal	-4.20	-2.82	1.38	0.2738572	0.709457
g16950	Pectin lyase fold/virulence factor, pectate lyase PLY/PYE-like, pectin lyase fold	0.47	-0.71	-1.17	0.2756634	0.709457
g8754	Cellulose/chitin-binding protein, N-terminal	2.74	0.76	-1.97	0.2773818	0.709457
g16623		6.27	5.00	-1.27	0.2780974	0.709457
g9543	EGF-like, conserved site, EGF-like domain	-3.54	-4.74	-1.20	0.2789354	0.709457
g17325	Acyl transferase/acyl hydrolase/lysophospholipase, lysophospholipase, catalytic domain	-3.60	-2.83	0.78	0.2803599	0.709457
g235	Cutinase/acetylxylan esterase, cutinase, monofunctional, alpha/beta hydrolase fold	0.37	1.02	0.65	0.2820881	0.709457
g4767	Galactose oxidase-like, early set domain, galactose oxidase, central domain superfamily, carbohydrate-binding WSC, immunoglobulin E-set, galactose oxidase/Kelch, beta propeller, immunoglobulin-like fold, glyoxal oxidase, N-terminal	-2.04	-1.13	0.92	0.2822151	0.709457
g11199	Class I glutamine amidotransferase-like, DJ-1/PpI	-1.50	-2.65	-1.16	0.2872811	0.717212
g16962	CW mannoprotein 1	2.73	2.25	-0.48	0.2963205	0.724674
g3965	Peptidase S10, serine carboxypeptidase, alpha/beta hydrolase fold, serine carboxypeptidase, serine active site, propeptide, carboxypeptidase Y	-3.04	-4.06	-1.02	0.296857	0.724674
g2649	CAP domain, Golgi-associated plant pathogenesis-related protein 1, SCP domain, cysteine-rich secretory protein-related, CAP superfamily	0.56	-0.05	-0.61	0.2969248	0.724674
g15939	Glycoside hydrolase family 11/12, glycoside hydrolase family 11, active site 1, glycosyl hydrolases family 11 (GH11) domain, concanavalin A-like lectin/glucanase domain superfamily, glycoside hydrolase family 11	5.91	6.59	0.69	0.2982773	0.724674
g9845	Glycoside hydrolase 131, catalytic N-terminal	3.11	2.60	-0.51	0.3065765	0.726461
g10911	Pectin lyase fold/virulence factor, pectate lyase, pectin lyase fold	1.50	0.60	-0.90	0.3066803	0.726461
g7852	Class I glutamine amidotransferase-like, DJ-1/PpI	2.19	0.69	-1.50	0.3070313	0.726461
g83	Domain of unknown function DUF1996	-3.82	-2.75	1.07	0.3076006	0.726461
g8701	Peptidase M14, carboxypeptidase A	0.22	-0.69	-0.92	0.3118827	0.726461
g9317	Transaldolase/fructose-6-phosphate aldolase, transaldolase type 1, transaldolase, active site, aldolase-type TIM barrel	0.89	1.97	1.07	0.3118933	0.726461
g183	Glycoside hydrolase superfamily, glycoside hydrolase, family 5	1.01	0.45	-0.57	0.3130606	0.726461
g12871	Thioredoxin domain, thioredoxin-like superfamily	-1.89	-2.41	-0.52	0.3242389	0.738856
g6139	Nucleoside diphosphate kinase, nucleoside diphosphate kinase-like domain superfamily, nucleoside diphosphate kinase-like domain, nucleoside diphosphate kinase, active site	-0.82	-0.18	0.64	0.3269327	0.738856
g3321	Glycoside hydrolase superfamily, chitinase II, chitinase insertion domain superfamily, endochitinase-like superfamily, glycoside hydrolase family 18, catalytic domain, chitin-binding, type 1, chitin-binding, type 1, conserved site	0.09	-0.96	-1.05	0.3296713	0.738856

continued on next page

Gene ID	IPR description	$\Delta cfr1-1$	WT	Log ₂ FC	P	Adjusted P
g4355	Pectin lyase fold/virulence factor, pectin lyase fold, pectate lyase superfamily protein	6.02	5.47	-0.55	0.330138	0.738856
g5029	Rhamnogalacturonan acetyltransferase RhgT-like, SGNH hydrolase-type esterase domain, SGNH hydrolase superfamily	0.80	1.67	0.88	0.3302845	0.738856
g9884	NADP-dependent oxidoreductase domain, NADP-dependent oxidoreductase domain superfamily, Aldo/keto reductase, conserved site	1.83	2.33	0.50	0.3306482	0.738856
g10729	Peptidase S10, serine carboxypeptidase, alpha/beta hydrolase fold	-1.27	-1.97	-0.70	0.3390225	0.748118
g6878	FERM/acyl-CoA-binding protein superfamily, acyl-CoA-binding protein, ACBP, acyl-CoA binding protein superfamily	0.25	-0.71	-0.96	0.3427245	0.748118
g4892	Glycoside hydrolase superfamily, glycoside hydrolase, family 5	6.09	5.50	-0.59	0.345224	0.748118
g12384	DinB/YitH-like putative metalloenzymes, protein of unknown function DUF1993	-2.98	-2.08	0.89	0.3464408	0.748118
g766	Cytochrome b5-like heme/steroid binding domain superfamily, FMN-dependent dehydrogenase, FMN hydroxy acid dehydrogenase domain, cytochrome b5-like heme/steroid binding domain, L-mandelate/L-lactate dehydrogenase, FMN-binding domain, aldolase-type TIM barrel, cytochrome b5, heme-binding site	-3.11	-2.26	0.85	0.3468607	0.748118
g6772	Glycosyl hydrolase, five-bladed beta-propeller domain superfamily	-3.05	-4.71	-1.66	0.3500043	0.748118
g923	Kre9/Krh1 family	1.15	1.71	0.56	0.3536252	0.748118
g8590	X8 domain, glycoside hydrolase superfamily, glucanoxyltransferase	4.08	4.80	0.72	0.3547154	0.748118
g8248	Aspartic peptidase A1 family, aspartic peptidase domain superfamily, peptidase family A1 domain, aspartic peptidase, active site, aspergillopepsin-like catalytic domain	-0.39	-1.17	-0.78	0.3567807	0.748118
g7590	Peptidase G1, peptidase G1 superfamily, concanavalin A-like lectin/glucanase domain superfamily	-0.30	1.09	1.40	0.3571294	0.748118
g12235	Glycoside hydrolase superfamily, glycoside hydrolase, family 5	-0.83	-1.50	-0.67	0.3575261	0.748118
g1171	Heat shock protein 70 kDa, C-terminal domain superfamily, heat shock protein 70 family, heat shock protein 70 kDa, conserved site, heat shock protein 70 kDa, peptide-binding domain superfamily, ATPase, nucleotide binding domain	0.65	1.70	1.05	0.3667201	0.755502
g9227	Carbohydrate-binding WSC	0.99	0.44	-0.55	0.3675109	0.755502
g7081	Chaperone DnaK, heat shock protein 70 kDa, peptide-binding domain superfamily, heat shock protein 70 family, ATPase, nucleotide binding domain, heat shock protein 70, conserved site, heat shock protein 70 kDa, C-terminal domain superfamily	-4.01	-3.36	0.65	0.3682586	0.755502
g3363	Chitinase insertion domain superfamily, endochitinase-like superfamily, chitinase II, LysM domain, glycoside hydrolase superfamily, glycoside hydrolase family 18, catalytic domain, chitin-binding, type 1, LysM domain superfamily, glycosyl hydrolases family 18 (GH18) active site, chitin-binding, type 1, conserved site	-0.99	-2.66	-1.67	0.3694029	0.755502
g6504	Tyrosinase copper-binding domain, uncharacterized domain, di-copper center	-0.53	0.05	0.58	0.372599	0.757757
g15857	Metallopeptidase, catalytic domain superfamily	0.62	-0.01	-0.63	0.3759913	0.760385
g16113	Beta-galactosidase/galacturonidase domain superfamily, glycosyl hydrolases family 2, sugar binding domain, glycoside hydrolase family 2, catalytic domain, glycoside hydrolase superfamily, glycoside hydrolase, family 2, immunoglobulin-like beta-sandwich, immunoglobulin-like fold, galactose-binding-like domain superfamily	1.08	0.59	-0.49	0.3782467	0.760696
g8231	Glycosyl hydrolase family 32, C-terminal, glycoside hydrolase, family 32, glycosyl hydrolase, five-bladed beta-propeller domain superfamily, glycoside hydrolase, family 32, active site, glycosyl hydrolase family 32, N-terminal, concanavalin A-like lectin/glucanase domain superfamily	2.93	3.65	0.72	0.4040737	0.792555
g11972	Glycosyl hydrolase family 53, glycoside hydrolase superfamily	1.36	2.06	0.70	0.4110335	0.792555
g16729	Glycosyl hydrolase, five-bladed beta-propeller domain superfamily, glycoside hydrolase, family 43	4.31	3.84	-0.47	0.4111883	0.792555
g13716	Glycoside hydrolase family 10 domain, cellulose-binding domain, fungal, cellulose-binding domain superfamily, glycoside hydrolase superfamily	-2.35	-1.94	0.41	0.4118721	0.792555
g3016	Peptidase, metallopeptidase, peptidase M12A, metallopeptidase, catalytic domain superfamily	6.20	6.67	0.47	0.4120394	0.792555
g4763	Glycosyl hydrolase family 32, C-terminal, glycosyl hydrolase family 32, N-terminal, glycosyl hydrolase, five-bladed beta-propeller domain superfamily, concanavalin A-like lectin/glucanase domain superfamily, glycoside hydrolase, family 32	1.35	1.74	0.38	0.4132277	0.792555
g13297		-2.12	-2.90	-0.78	0.4135067	0.792555
g14816	Metallo-beta-lactamase, ribonuclease Z/Hydroxycyglutathione hydrolase-like	-1.49	-0.95	0.54	0.4137677	0.792555
g15867	Alpha/beta hydrolase fold-1, alpha/beta hydrolase fold, peptidase S33 tripeptidyl aminopeptidase-like, C-terminal	-1.85	-1.24	0.60	0.4139212	0.792555
g555	Thioredoxin-like superfamily, protein disulfide isomerase, disulfide isomerase, thioredoxin domain, thioredoxin, conserved site	0.91	1.37	0.45	0.4159819	0.792555
g6631	Glycoside hydrolase family 17, glycoside hydrolase superfamily	-2.30	-2.96	-0.66	0.4228366	0.798634
g4476	Peptidase family A1 domain, aspartic peptidase domain superfamily, aspartic peptidase A1 family, aspergillopepsin-like catalytic domain, aspartic peptidase, active site	-4.05	-3.27	0.78	0.4235847	0.798634
g3073	Pectin lyase fold/virulence factor, pectin lyase fold, glycoside hydrolase, family 28, parallel beta-helix repeat	2.74	1.36	-1.39	0.4299316	0.800784

continued on next page

Gene ID	IPR description	Δ cd1-1	WT	Log ₂ FC	P	Adjusted P
g1020	S-adenosylmethionine synthetase superfamily, S-adenosylmethionine synthetase, central domain, S-adenosylmethionine synthetase, conserved site, S-adenosylmethionine synthetase, S-adenosylmethionine synthetase, C-terminal, S-adenosylmethionine synthetase, N-terminal	-2.98	-2.01	0.97	0.4302418	0.800784
g3990	Concanavalin A-like lectin/glucanase domain superfamily, glycoside hydrolase family 16	0.52	0.97	0.45	0.4317905	0.800784
g13513	Cellulose-binding domain, fungal, cellulose-binding domain superfamily	-3.99	-3.39	0.61	0.4340334	0.800784
g13614	Cellulose-binding domain, fungal, cellulose-binding domain superfamily	-1.63	-2.30	-0.66	0.4357856	0.800784
g16649	SGNH hydrolase superfamily, GDSL lipase/esterase	-1.17	-2.37	-1.19	0.4415339	0.803507
g8761	Glycoside hydrolase, family 28, pectin lyase fold, pectin lyase fold/virulence factor	0.99	0.49	-0.50	0.4417067	0.803507
g14481	Cyclin-like, palmitoyl protein thioesterase, cyclin-like superfamily, cyclin/cyclin-like subunit Sn8, alpha/beta hydrolase fold, cyclin, N-terminal	-2.39	-1.77	0.62	0.4508535	0.814020
g11320	Tetratricopeptide-like helical domain superfamily, CHAT domain	-2.68	-1.98	0.70	0.4519836	0.814020
g16195	Endonuclease/exonuclease/phosphatase superfamily	-1.61	-2.28	-0.67	0.4600422	0.822299
g6459	WD40/YVTN repeat-like-containing domain superfamily, cytochrome cd1-nitrite reductase-like, haem d1 domain superfamily, lactonase, 7-bladed beta propeller	-3.99	-3.13	0.86	0.463385	0.822299
g14329	Carboxylesterase type B, conserved site, alpha/beta hydrolase fold, carboxylesterase type B, active site, carboxylesterase, type B	2.76	3.17	0.41	0.464622	0.822299
g6295	Protein of unknown function DUF3455	1.66	0.91	-0.75	0.4669821	0.822299
g15989	Armadillo-like helical, ribosomal protein L19/L19e, Gcn1, N-terminal, ribosomal protein L19/L19e superfamily, ribosomal protein L19/L19e, domain 1, ribosomal protein L19, eukaryotic, Armadillo-type fold, translational activator Gcn1, Parkin co-regulated protein, HEAT, type 2, TOG domain, ribosomal protein L19/L19e conserved site	4.47	4.87	0.40	0.471606	0.822299
g16857	Peptidase family A1 domain, aspartic peptidase domain superfamily, aspartic peptidase A1 family	-3.17	-2.54	0.62	0.4730543	0.822299
g12195	Glycoside hydrolase family 16, concanavalin A-like lectin/glucanase domain superfamily	-3.71	-2.61	1.10	0.4731133	0.822299
g3972	Glycoside hydrolase family 16, concanavalin A-like lectin/glucanase domain superfamily	0.88	1.34	0.46	0.4749172	0.822299
g12093	Glycoside hydrolase family 16, concanavalin A-like lectin/glucanase domain superfamily	-1.14	-0.50	0.63	0.4770245	0.822299
g14024	Leucine-rich repeat domain superfamily	-1.03	-0.52	0.51	0.480106	0.823667
g8504	Protein of unknown function DUF3455	-0.57	-1.28	-0.71	0.4836094	0.823667
g14243	Armadillo-like helical, ribosomal protein L19/L19e, Gcn1, N-terminal, ribosomal protein L19/L19e superfamily, ribosomal protein L19/L19e, domain 1, ribosomal protein L19, eukaryotic, Armadillo-type fold, translational activator Gcn1, Parkin co-regulated protein, HEAT, type 2, TOG domain, ribosomal protein L19/L19e conserved site	-0.50	0.91	1.42	0.4846441	0.823667
g12277	Alpha/beta hydrolase fold, carboxylesterase type B, active site, carboxylesterase, type B	-0.17	-0.72	-0.55	0.4869693	0.823752
g15710	Peptidase S8/S53 domain, peptidase S8, subtilisin, His-active site, peptidase S8/S53 domain superfamily, peptidase S8, subtilisin-related, peptidase S8 propeptide/proteinase inhibitor I9, superfamily	-1.16	-0.75	0.42	0.4898506	0.824772
g16104	Peptidase S8/S53 domain, peptidase S8, subtilisin, His-active site, peptidase S8/S53 domain superfamily, peptidase S8, subtilisin-related, peptidase S8 propeptide/proteinase inhibitor I9, superfamily	6.16	5.70	-0.46	0.4938612	0.825399
g8486	Beta-hexosaminidase, eukaryotic type, N-terminal, glycoside hydrolase family 20, catalytic domain, beta-hexosaminidase, beta-hexosaminidase-like, domain 2, glycoside hydrolase superfamily	-2.44	-1.75	0.69	0.4957645	0.825399
g519	EF-hand domain pair, EF-hand domain, EF-Hand 1, calcium-binding site, calmodulin	-0.47	-1.43	-0.96	0.4970635	0.825399
g4593	NodB homology domain, glycoside hydrolase/deacetylase, beta/alpha barrel	5.35	4.25	-1.10	0.5007726	0.827761
g6835	Pex, N-terminal, glycoside hydrolase family 16, carbohydrate-binding WSC, zinc finger, RING/FYVE/PHD-type, peroxisome assembly protein 12, concanavalin A-like lectin/glucanase domain superfamily	0.00	0.38	0.38	0.5110129	0.840848
g15003	Alpha/beta hydrolase fold, esterase, PHB depolymerase	1.29	1.68	0.39	0.5148587	0.843343
g16906	Alpha/beta hydrolase fold, tannase/feruloyl esterase	-1.78	-2.57	-0.79	0.5232098	0.849087
g5013	Peptidase M14, carboxypeptidase A	5.19	4.54	-0.65	0.5236172	0.849087
g11706	Peptidase S8 propeptide/proteinase inhibitor I9 superfamily	2.54	2.12	-0.42	0.5270801	0.849087
g4777	Dimeric alpha-beta barrel, antibiotic biosynthesis monooxygenase domain	3.74	3.02	-0.72	0.5285399	0.849087
g7610	Cupredoxin, multicopper oxidase, type 3, multicopper oxidases, conserved site, multicopper oxidase, type 1, multicopper oxidase, copper-binding site, multicopper oxidase type 2	-3.73	-3.14	0.59	0.5300928	0.849087
g6361	Galactose oxidase/Kelch, beta propeller, Kelch-type beta propeller	-0.94	-0.59	0.36	0.5330418	0.850049
g900	Galactose oxidase/Kelch, beta propeller, Kelch-type beta propeller	-3.48	-2.94	0.54	0.5398777	0.857174

continued on next page

Gene ID	IPR description	$\Delta cfr1-1$	WT	\log_2FC	P	Adjusted P
g12817		-4.83	-4.40	0.43	0.5463766	0.863704
g10240	Alpha carbonic anhydrase domain, alpha carbonic anhydrase domain superfamily, carbonic anhydrase, prokaryotic-like, carbonic anhydrase, alpha class	1.70	1.33	-0.37	0.5557039	0.874630
g9271	Ubiquitin-like domain superfamily, ubiquitin conserved site, ubiquitin-like domain, ubiquitin domain	-1.21	-0.91	0.29	0.5660071	0.886989
g10632	Phytanoyl-CoA dioxygenase	-2.99	-2.47	0.52	0.5712113	0.891287
g7682		-2.26	-1.88	0.39	0.5770507	0.894970
g2502		3.41	3.17	-0.24	0.5785167	0.894970
g13805	Protein of unknown function DUF3455	2.66	1.98	-0.68	0.5819387	0.896433
g1220		-2.91	-2.32	0.59	0.5863654	0.897274
g11415	Signaling mucin M5B2	1.59	1.93	0.34	0.5896649	0.897274
g9319	Superoxide dismutase, copper/zinc binding site, superoxide dismutase (Cu/Zn)/ superoxide dismutase copper chaperone, superoxide dismutase, copper/zinc binding domain, superoxide dismutase-like, copper/zinc binding domain superfamily	2.09	1.78	-0.31	0.5913067	0.897274
g10601	Aldo/keto reductase, Aldo/keto reductase, conserved site, NADP-dependent oxidoreductase domain, NADP-dependent oxidoreductase domain superfamily	-0.95	-1.25	-0.31	0.5951976	0.897274
g8790	Peptidase M28	4.52	4.11	-0.41	0.5956024	0.897274
g17816	Glycoside hydrolase, family 27, galactose-binding-like domain superfamily, alpha galactosidase, C-terminal beta sandwich domain, glycosyl hydrolase, all-beta, glycoside hydrolase superfamily, aldolase-type TIM barrel	2.22	2.75	0.54	0.5973565	0.897274
g7410	SGNH hydrolase-type esterase domain, SGNH hydrolase superfamily	7.64	7.86	0.22	0.6002149	0.897842
g11761	Aspartic peptidase domain superfamily, aspartic peptidase A1 family, aspartic peptidase, active site, peptidase family A1 domain	-1.31	-0.99	0.31	0.6120275	0.911256
g14799	Glycoside hydrolase family 10 domain, glycoside hydrolase superfamily	1.46	1.06	-0.40	0.620129	0.911256
g11136	FAD-linked oxidase, N-terminal, FAD-binding, type PCMH-like superfamily, FAD-binding domain, PCMH-type	7.03	6.77	-0.26	0.6211413	0.911256
g10913	Isochorismatase-like, isochorismatase-like superfamily	-1.19	-1.52	-0.32	0.6225341	0.911256
g13290		-4.03	-3.56	0.48	0.6252037	0.911256
g10055	Sialidase superfamily	6.56	6.28	-0.28	0.6276629	0.911256
g1204	FAD/NAD(P)-binding domain superfamily, thioredoxin reductase, pyridine nucleotide- disulfide oxidoreductase, class II, active site, FAD/NAD(P)-binding domain, vacuolar protein sorting-associated protein 53, Vps53-like, N-terminal	-0.20	-1.31	-1.10	0.6292667	0.911256
g11945		2.13	1.65	-0.48	0.6293563	0.911256
g12780	WD40/YVTN repeat-like-containing domain superfamily	1.98	1.68	-0.30	0.6351775	0.911256
g7792	Peptidase M28, M28 Zn-peptidase glutamyl cyclase	-1.52	-1.17	0.36	0.6428047	0.911256
g10659	Sec7 domain, Armadillo-type fold, Sec7, C-terminal domain superfamily, Mon2, dimerization and cytoplasm-binding domain, Sec7, C-terminal, guanine nucleotide exchange factor, N-terminal, Sec7 domain superfamily	-2.68	-3.09	-0.41	0.6428154	0.911256
g9512	Nuclear transport factor 2, eukaryote, nuclear transport factor 2, NTF2-like domain superfamily	-3.00	-2.60	0.40	0.6437767	0.911256
g5053	Alpha/beta hydrolase fold, peptidase S9, prolyl oligopeptidase, catalytic domain	0.41	-0.02	-0.43	0.6473106	0.911256
g1631	Concanavalin A-like lectin/glucanase domain superfamily, glycoside hydrolase family 16	1.35	1.03	-0.31	0.6480492	0.911256
g6181	Necrosis-inducing protein	4.17	3.97	-0.20	0.6489888	0.911256
g12201	Lysophospholipase, catalytic domain, glycoside hydrolase superfamily, acyl transferase/acyl hydrolase/lysophospholipase	0.29	-0.18	-0.46	0.6494589	0.911256
g4080		2.86	3.16	0.29	0.6536824	0.913641
g1291	Aldehyde dehydrogenase domain, aldehyde dehydrogenase, C-terminal, aldehyde dehydrogenase, N-terminal, aldehyde dehydrogenase, glutamic acid active site, aldehyde dehydrogenase, cysteine active site, aldehyde/histidinol dehydrogenase	0.13	-0.11	-0.24	0.6562147	0.913653
g12967	Alpha/beta hydrolase fold-1, alpha/beta hydrolase fold	4.68	4.93	0.25	0.6611626	0.915406
g15019	Zinc finger, MYND-type, alpha/beta hydrolase fold, cutinase/acetylxylan esterase	5.29	5.60	0.31	0.6625312	0.915406
g15861		0.85	0.56	-0.29	0.6657488	0.916354
g390	FKBP-type peptidyl-prolyl cis-trans isomerase domain	-2.12	-2.55	-0.43	0.6776924	0.925858

continued on next page

Gene ID	IPR description	$\Delta\text{cdr1-1}$	WT	Log_2FC	P	Adjusted P
g1027	Kre9/Knh1 family	3.61	4.17	0.56	0.6805968	0.925858
g11276	PA domain, peptidase M28, SGAP-like	2.11	1.76	-0.35	0.6873121	0.925858
g7350	Pectin lyase fold, parallel beta-helix repeat, glycoside hydrolase, family 28, pectin lyase fold/virulence factor	1.95	2.19	0.24	0.6877679	0.925858
g13053	Haem peroxidase, fungal ligninase, peroxidase, active site, haem peroxidase superfamily	-2.73	-3.04	-0.31	0.689261	0.925858
g12382	S-adenosyl-L-methionine-dependent methyltransferase, methyltransferase domain 25	-3.16	-3.53	-0.37	0.6916188	0.925858
g936	Ribosome maturation protein SBD5, N-terminal domain superfamily, ribosome maturation protein SBD5, N-terminal, ribosome maturation protein Sdo1/SBD5-like	-2.87	-2.53	0.34	0.6918295	0.925858
g2478		3.64	3.44	-0.19	0.6959669	0.925858
g9067	Serine/threonine-protein kinase TOR, FATC domain, PIK-related kinase FAT, Armadillo-type fold, FKBP12-rapamycin binding domain, Armadillo-like helical, phosphatidylinositol 3-/4-kinase, catalytic domain superfamily, phosphatidylinositol 3-/4-kinase, conserved site, FKBP12-rapamycin binding domain superfamily, protein kinase-like domain superfamily, phosphatidylinositol 3-/4-kinase, catalytic domain, domain of unknown function DUF3385, target of rapamycin protein, PIK-related kinase	-1.19	-1.47	-0.28	0.69863	0.925858
g4585	Amidase, amidase signature domain, amidase signature (A5) superfamily	3.52	3.28	-0.24	0.7020469	0.925858
g7515	Kelch-type beta propeller, Kelch repeat type 1	-1.44	-1.67	-0.23	0.704676	0.925858
g15722	Pectate lyase, pectin lyase fold/virulence factor, pectin lyase fold	-0.85	-1.05	-0.20	0.7063003	0.925858
g14893	Peptidase M43, pregnancy-associated plasma-A, metallopeptidase, catalytic domain superfamily	0.33	0.58	0.25	0.7072016	0.925858
g6817		1.57	1.30	-0.28	0.7136497	0.925858
g1621	Peptidase S8 propeptide/proteinase inhibitor I9, peptidase S8, subtilisin-related, peptidase S8 propeptide/proteinase inhibitor I9 superfamily, peptidase S8/S53 domain superfamily, peptidase S8, subtilisin, His-active site, proteinase K-like catalytic domain, peptidase S8, subtilisin, Ser-active site	-2.26	-2.50	-0.24	0.7148287	0.925858
g6251	Glycoside hydrolase, family 61	1.53	0.87	-0.66	0.7149224	0.925858
g13864	RlpA-like domain superfamily	1.71	2.02	0.31	0.7161332	0.925858
g6145	Domain of unknown function DUF1996	2.44	2.16	-0.28	0.720075	0.926109
g16949	Peptidase S8/S53 domain superfamily, peptidase S8, subtilisin-related, peptidase S8/S53 domain, peptidase S8 propeptide/proteinase inhibitor I9 superfamily, peptidase S8, subtilisin, His-active site, proteinase K-like catalytic domain, peptidase S8, subtilisin, Ser-active site, peptidase S8, subtilisin, His-active site	0.29	0.55	0.25	0.7214442	0.926109
g9676	RNA recognition motif domain, RNA-binding domain superfamily, nucleotide-binding alpha-beta plat domain superfamily	0.19	0.40	0.20	0.7287915	0.929303
g1961	Alpha/beta hydrolase fold, carboxylesterase type B, active site, carboxylesterase, type B	5.05	4.86	-0.19	0.7302999	0.929303
g15912		4.40	4.66	0.26	0.7326033	0.929303
g786	Translation elongation factor EF1B, beta/delta subunit, guanine nucleotide exchange domain, translation elongation factor EF1B, beta/delta chains, conserved site, translation elongation factor eEF-1beta-like superfamily, glutathione S-transferase, C-terminal domain superfamily, translation elongation factor EF1B/ribosomal protein S6, elongation factor 1 beta, central acidic region, eukaryote	-1.68	-1.38	0.30	0.7342011	0.929303
g3852	P-loop containing nucleoside triphosphate hydrolase, ATPase, F1/V1/A1 complex, alpha/beta subunit, nucleotide-binding domain, ATP synthase alpha/beta subunit, N-terminal extension, ATP synthase subunit alpha, N-terminal domain-like superfamily, ATPase, F1/V1/A1 complex, alpha/beta subunit, N-terminal domain, V-type ATP synthase catalytic alpha chain, ATPase, F1/V1/A1 complex, alpha/beta subunit, N-terminal domain superfamily, ATPase, V1 complex, subunit A, ATPase, alpha/beta subunit, nucleotide-binding domain, active site, ATPase, F1/V1 complex, beta/alpha subunit, C-terminal	-3.23	-2.97	0.26	0.7404022	0.933887
g5020	Endonuclease/exonuclease/phosphatase superfamily, endonuclease/exonuclease/phosphatase	0.69	0.91	0.23	0.7590932	0.948523
g5140	Alpha/beta hydrolase fold, carboxylesterase, type B	5.05	5.19	0.13	0.7619345	0.948523
g4369	Glycoside hydrolase, family 3, N-terminal, glycoside hydrolase family 3 C-terminal domain superfamily, immunoglobulin-like fold, glycoside hydrolase family 3 C-terminal domain, glycoside hydrolase, family 3, N-terminal domain superfamily, Fibronectin type III-like domain, glycoside hydrolase, family 3, active site, glycoside hydrolase superfamily	3.59	3.45	-0.14	0.7643657	0.948523
g7743	Glycoside hydrolase family 17, glycoside hydrolase superfamily	1.73	1.50	-0.23	0.7644574	0.948523
g2494		3.80	3.96	0.16	0.7672871	0.948523
g15891	Alpha/beta hydrolase fold, carboxylesterase type B, active site, carboxylesterase, type B, carboxylesterase type B, conserved site	-0.18	0.07	0.25	0.7694842	0.948523
g8260		-1.64	-2.08	-0.44	0.7735137	0.948523

continued on next page

Gene ID	IPR description	$\Delta cfr1-1$	WT	Log ₂ FC	P	Adjusted P
g563	Glycosyl hydrolase, five-bladed beta-propeller domain superfamily, carbohydrate binding module family 6, galactose-binding-like domain superfamily, cellulose binding, type IV, glycoside hydrolase, family 43	-2.16	-2.35	-0.18	0.7748653	0.948523
g12121	Glycosyl hydrolase, five-bladed beta-propeller domain superfamily, carbohydrate binding module family 6, galactose-binding-like domain superfamily, cellulose binding, type IV, glycoside hydrolase, family 43	-0.17	0.19	0.36	0.7779458	0.948523
g4480	Alpha/beta hydrolase fold, alpha/beta hydrolase fold-1	3.69	3.96	0.27	0.7795188	0.948523
g8214	Cupredoxin, multicopper oxidase, copper-binding site, fungal multicopper oxidase, cupredoxin domain 3, multicopper oxidase, type 3, multicopper oxidase, type 3, multicopper oxidase, conserved site, multicopper oxidase, type 1	-0.72	-1.08	-0.36	0.7808286	0.948523
g8296	Berberine/berberine-like, FAD-linked oxidase, N-terminal, FAD-binding domain, PCMH-type, FAD-binding, type PCMH-like superfamily	7.77	7.62	-0.16	0.7847469	0.948893
g10261	Histidine phosphatase superfamily, histidine phosphatase superfamily, clade 1	-3.98	-3.78	0.20	0.7863753	0.948893
g8677	Protein of unknown function DUF1348, NTF2-like domain superfamily	-2.29	-2.47	-0.18	0.7910692	0.949646
g13282	Protein of unknown function DUF1348, NTF2-like domain superfamily	-3.74	-3.40	0.35	0.7924617	0.949646
g9786	MmgE/PrpD, MmgE/PrpD superfamily, 2-methylcitrate dehydratase PrpD, MmgE/PrpD superfamily, domain 2, MmgE/PrpD superfamily, domain	1.69	1.49	-0.20	0.7948692	0.949646
g17881	Glycoside hydrolase family 16, glycoside hydrolase, family 16, CRH1, predicted, concanavalin A-like lectin/glucanase domain superfamily	1.15	1.35	0.20	0.7999718	0.952598
g11805	UROD/MetE-like superfamily, cobalamin-independent methionine synthase, cobalamin-independent methionine synthase MetE, N-terminal, cobalamin-independent methionine synthase MetE, C-terminal/archaeal	-2.40	-2.73	-0.33	0.8125792	0.961358
g4570	Glycoside hydrolase, family 43, Alpha-L-arabinofuranosidase, glycosyl hydrolase, five-bladed beta-propeller domain superfamily	-1.78	-1.63	0.15	0.8126395	0.961358
g16861	Glycoside hydrolase, family 43, Alpha-L-arabinofuranosidase, glycosyl hydrolase, five-bladed beta-propeller domain superfamily	2.30	2.58	0.28	0.8160695	0.962271
g14975	Pectin lyase fold, glycoside hydrolase, family 28, pectin lyase fold/virulence factor, parallel beta-helix repeat	1.01	1.33	0.32	0.820206	0.963335
g13481	Pectin lyase fold, glycoside hydrolase, family 28, pectin lyase fold/virulence factor, parallel beta-helix repeat	1.12	1.37	0.25	0.8222946	0.963335
g17120	5'-Nucleotidase, C-terminal domain superfamily, 5'-nucleotidase, C-terminal, metallo-dependent phosphatase-like, calcineurin-like phosphoesterase domain, ApaH type, 5'-nucleotidase/apyrase	0.91	0.76	-0.15	0.8252096	0.963377
g8638	5'-Nucleotidase, C-terminal domain superfamily, 5'-nucleotidase, C-terminal, metallo-dependent phosphatase-like, calcineurin-like phosphoesterase domain, ApaH type, 5'-nucleotidase/apyrase	-3.83	-4.03	-0.20	0.8339967	0.963377
g452	SUN family	3.45	3.29	-0.16	0.8346998	0.963377
g7601	Cytochrome b5-like heme/steroid binding domain, succinate dehydrogenase/fumarate reductase flavoprotein, catalytic domain superfamily, cytochrome b5-like heme/steroid binding domain superfamily, FAD-dependent oxidoreductase 2, FAD-binding domain, flavocytochrome c, FAD/NAD(P)-binding domain superfamily	-2.05	-1.86	0.19	0.8351617	0.963377
g7052	Peptidase S16, active site, PUA-like superfamily, peptidase S16, Lon, proteolytic domain, Lon, substrate-binding domain, ribosomal protein S5 domain 2-type fold, ATPase, AAA-type, core, Lon protease homolog, chloroplast/mitochondrial, Lon protease, bacterial/eukaryotic-type, ribosomal protein S5 domain 2-type fold, subgroup, AAA+ ATPase domain, Lon protease, P-loop containing nucleoside triphosphate hydrolase	-1.64	-1.43	0.21	0.8382785	0.963377
g17239	Catalase-peroxidase haem, haem peroxidase, haem peroxidase superfamily, peroxidase, active site, peroxidase:haem-ligand binding site	4.15	4.27	0.12	0.8382978	0.963377
g16905	Uncharacterized protein family UPP0311	3.22	3.07	-0.14	0.8430929	0.964348
g223	Autophagy-related protein 27	-3.70	-3.90	-0.19	0.84528	0.964348
g12827	Endochitinase-like superfamily, chitinase II, glycoside hydrolase family 18, catalytic domain, chitin-binding, type 1, glycoside hydrolase superfamily	7.85	8.00	0.15	0.8536368	0.964348
g17201	Alpha-L-arabinofuranosidase B, arabinose-binding domain, alpha-L-arabinofuranosidase B, catalytic, alpha-L-arabinofuranosidase B, arabinose-binding domain superfamily, concanavalin A-like lectin/glucanase domain superfamily, alpha-L-arabinofuranosidase B	5.20	5.10	-0.10	0.8542373	0.964348
g14035	Glucanoyltransferase, glycoside hydrolase superfamily	0.44	0.54	0.10	0.8550702	0.964348
g12925	Cellulose-binding domain, fungal, glycoside hydrolase, family 45, cellulose-binding domain superfamily, RlpA-like domain superfamily	2.67	2.54	-0.13	0.8551262	0.964348
g4431	Peptidase M28, SCAP-like, peptidase M28, PA domain	-2.50	-2.39	0.12	0.8579853	0.964567
g10876	Glycoside hydrolase, family 61	0.51	0.38	-0.13	0.8665244	0.967102
g10917	Phospholipase A2 domain superfamily, phospholipase A2, prokaryotic/fungal	3.86	3.78	-0.08	0.8672044	0.967102
g17675	Glycosyl hydrolase, five-bladed beta-propeller domain superfamily, glycosyl hydrolase family 32, C-terminal, glycosyl hydrolase family 32, N-terminal, concanavalin A-like lectin/glucanase domain superfamily, glycoside hydrolase, family 32	-2.76	-2.62	0.14	0.8682545	0.967102
g9447	Glycosyl hydrolase, five-bladed beta-propeller domain superfamily, glycosyl hydrolase family 32, C-terminal, glycosyl hydrolase family 32, N-terminal, concanavalin A-like lectin/glucanase domain superfamily, glycoside hydrolase, family 32	-1.26	-1.36	-0.10	0.876335	0.969663
g4900	FAD-linked oxidase, N-terminal, FAD-binding, type PCMH-like superfamily, FAD-binding domain, PCMH-type, berberine/berberine-like	-1.71	-1.60	0.11	0.876633	0.969663

continued on next page

Gene ID	IPR description	$\Delta\text{cdr1-1}$	WT	Log ₂ FC	P	Adjusted P
g16730	Glycoside hydrolase, family 43, glycosyl hydrolase, five-bladed beta-propeller domain superfamily, glycoside hydrolase, family 43, endo-1, 5-alpha-L-arabinosidase	1.84	1.92	0.07	0.876081	0.969683
g3863		-0.84	-0.92	-0.08	0.8817623	0.970207
g1468		-0.53	-0.67	-0.14	0.8883246	0.974465
g6907	FKBP-type peptidyl-prolyl cis-trans isomerase domain	1.22	1.15	-0.07	0.8928558	0.976477
g4291		-0.03	0.15	0.18	0.8992575	0.980516
g8359	Glycoside hydrolase, family 61	0.85	0.95	0.10	0.9021451	0.980710
g14769	Six-hairpin glycosidase-like superfamily, carbohydrate binding module family 20, glucoamylase, carbohydrate-binding-like fold, six-hairpin glycosidase superfamily, glucoamylase, starch-binding, GH15-like domain, immunoglobulin-like fold	0.22	-0.02	-0.24	0.9085319	0.983856
g450	Aldolase-type TIM barrel, glycoside hydrolase superfamily, glycoside hydrolase family GH114, TIM barrel domain	-1.23	-1.14	0.09	0.9137613	0.983856
g16746	Galactose-binding-like domain superfamily, beta-glucuronidase, C-terminal, six-hairpin glycosidase-like superfamily, alpha-L-rhamnosidase, six-hairpin glycosidase domain, glycoside hydrolase superfamily, six-hairpin glycosidase superfamily	4.16	4.05	-0.11	0.9143255	0.983856
g8785	Tyrosinase copper-binding domain, uncharacterized domain, di-copper center	0.88	0.75	-0.13	0.9159097	0.983856
g16097	CAP superfamily, CAP domain, cysteine-rich secretory protein-related, Golgi-associated plant pathogenesis-related protein 1, SCP domain	3.68	3.63	-0.05	0.9218284	0.987284
g15470	Glycosyl hydrolase, five-bladed beta-propeller domain superfamily, glycosyl hydrolase family 32, N-terminal, glycosyl hydrolase family 32, C-terminal, glycoside hydrolase, family 32, concanavalin A-like lectin/galactanase domain superfamily	-3.09	-2.92	0.17	0.9263663	0.989217
g12126	Glycosyl hydrolase, family 88, six-hairpin glycosidase superfamily, six-hairpin glycosidase-like superfamily	-0.61	-0.56	0.05	0.9298667	0.990034
g4263	Triosephosphate isomerase, triosephosphate isomerase, active site, aldolase-type TIM barrel, triosephosphate isomerase superfamily, triosephosphate isomerase, bacterial/eukaryotic	-1.12	-1.05	0.07	0.933194	0.990496
g7674	Complex I intermediate-associated protein 30, mitochondrial, NADH:ubiquinone oxidoreductase intermediate-associated protein 30, galactose-binding-like domain superfamily	2.79	2.75	-0.04	0.9357727	0.990496
g12240	Chitinase insertion domain superfamily, chitinase II, glycoside hydrolase family 18, catalytic domain, glycoside hydrolase superfamily	4.45	4.50	0.05	0.9453009	0.996426
g10854	FAD-binding domain, PCMH-type, FAD-linked oxidase, N-terminal, FAD-binding, type PCMH-like superfamily, berberine-like, FAD-binding, type PCMH, subdomain 2, FAD-binding, type PCMH, subdomain 1	-3.82	-3.75	0.07	0.9473665	0.996426
g17018		-2.17	-2.13	0.04	0.9549585	0.996426
g8818	Peptidase S10, serine carboxypeptidase, serine carboxypeptidases, histidine active site, alpha/beta hydrolase fold, serine carboxypeptidase, serine active site	3.87	3.92	0.05	0.9552146	0.996426
g17204	SMP-30/gluconolactonase/LRE-like region, six-bladed beta propeller, TolB-like	-1.64	-1.60	0.04	0.9602864	0.996426
g9171	Glycoside hydrolase, family 5, glycoside hydrolase superfamily	3.19	3.23	0.05	0.963219	0.996426
g10884	Peptidase family A1 domain, aspartic peptidase domain superfamily, aspartic peptidase A1 family	1.47	1.50	0.03	0.9680415	0.996426
g15794	Cutinase/acetylxylan esterase, alpha/beta hydrolase fold, cutinase, monofunctional	1.88	1.87	-0.02	0.9733306	0.996426
g6847	Phytocyanin domain, cupredoxin	-2.27	-2.29	-0.02	0.9745632	0.996426
g16281		-1.32	-1.28	0.04	0.9748903	0.996426
g15816	Chloroperoxidase-like superfamily, chloroperoxidase	4.63	4.66	0.03	0.9794859	0.996426
g4544	PA14/GLEYA domain, GLEYA adhesin domain	-0.57	-0.54	0.03	0.9795649	0.996426
g7572	SGNH hydrolase-type esterase domain, SGNH hydrolase superfamily	-0.32	-0.33	-0.02	0.980325	0.996426
g4411		-1.46	-1.48	-0.02	0.9804546	0.996426
g2339	Haem peroxidase, catalase-peroxidase haem, haem peroxidase superfamily, peroxidase, active site, peroxidases haem-ligand binding site	1.15	1.17	0.02	0.9912574	0.996426
g7868	Glucoamylase, glucoamylase, CBM20 domain, carbohydrate binding module family 20, six-hairpin glycosidase-like superfamily, immunoglobulin-like fold, six-hairpin glycosidase superfamily, glucoamylase, starch-binding, GH15-like domain, carbohydrate-binding-like fold	6.71	6.72	0.01	0.9916505	0.996426
g17213	Cellulose-binding domain, fungal, cellulose-binding domain superfamily, glycoside hydrolase, family 61	1.27	1.25	-0.01	0.9918143	0.996426
g805	Rhamnolacturonan lyase, domain III, rhamnolacturonase B, rhamnolacturonase B, N-terminal, galactose-binding-like domain superfamily, rhamnolacturonan lyase, domain II, glycoside hydrolase-type carbohydrate-binding, carbohydrate-binding-like fold, galactose mutarotase-like domain superfamily	0.92	0.91	-0.01	0.9923427	0.996426
g6411	Formin, GTPase-binding domain, formin, FH2 domain superfamily, Armadillo-like helical, formin, FH2 domain, formin, FH3 domain, Diaphanous	0.80	0.79	-0.01	0.9936736	0.996426
g14330	Glycoside hydrolase, family 16, CRH1, predicted, glycoside hydrolase family 16, concanavalin A-like lectin/galactanase domain superfamily	1.18	1.18	0.00	0.9977725	0.997772

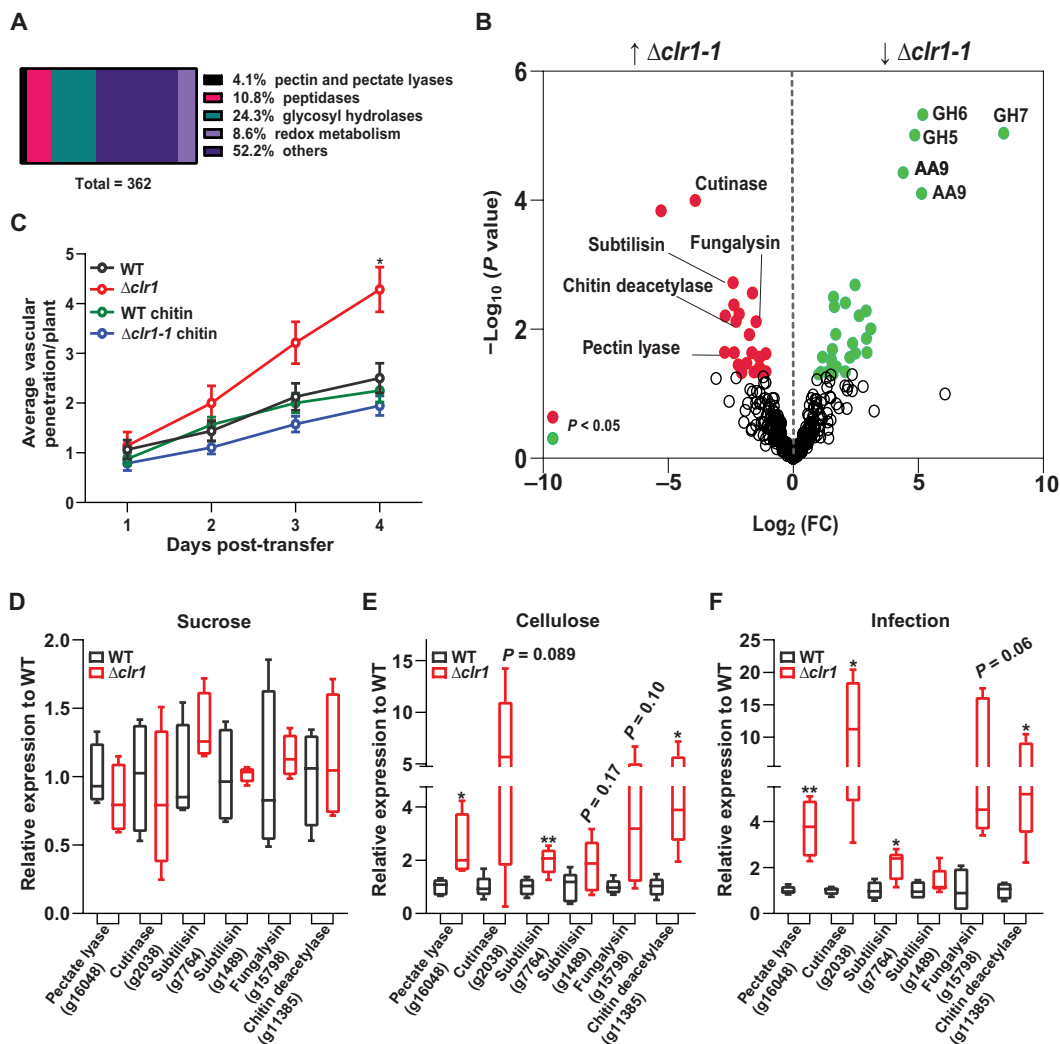


Fig. 5. Secreted virulence factors are up-regulated in $\Delta clr1-1$ during Arabidopsis root infection. (A) Percentages of the most representative family proteins identified in the secretome of WT Fo at 3 dpt of seedlings in hydroponics. (B) Volcano plot of differences in the abundance of proteins identified in the secretome of $\Delta clr1-1$ relative to WT. Proteins significantly (moderated t test, $P < 0.05$) less or more present in the $\Delta clr1-1$ secretome are shown in green or red, respectively. $N = 4$ biological replicates. The name or family of the most relevant proteins is indicated. (C) Cumulative Arabidopsis root vascular penetration by Fo at different dpt to WT or $\Delta clr1-1$ hyphae-containing plates. Half of the plants were pretreated with chitin. Values are means \pm SEM, $N \geq 14$ from one representative experiment. The experiment was repeated three times with similar results. RM two-way ANOVA on vascular penetration rate: $P < 0.001$ (fungal genotype and treatment), $P < 0.0001$ (time), $P < 0.0001$ (fungal genotype \times time). Tukey's multiple comparisons test; * $P < 0.05$ with respect to WT at 4 dpt. (D to F) Gene expression of virulence factors relative to *FoTub* in WT or $\Delta clr1-1$ grown 3 days in sucrose (D) or cellulose (E) or at 3 dpt in Arabidopsis roots (F). The genes were selected among the ones enriched in the $\Delta clr1-1$ secretome as in (B): pectate lyase (g16048), cutinase (g2038), subtilisins (g7764 and g1489), fungalsin (g15798), and chitin deacetylase (g11385). Box plots: Centerlines show the medians; box limits indicate the 25th and 75th percentiles; whiskers extend to the minimum and maximum, $N \geq 4$. For each gene, the data were normalized to WT. Welch's unpaired t test; * $P < 0.05$. ** $P < 0.01$. Smaller P values are indicated.

The role of CLR1 in Fo infection is conserved among different pathosystems

The Fo species complex contains different host-specific plant pathogens, for some of which we also found CLR1 orthologs with a protein sequence similarity of 95.69% with the Fo5176 CLR1 and the same DNA binding sequence (Fig. 1, A and B). Thus, we asked whether the increased virulence displayed by $\Delta clr1-1$ in the Arabidopsis-Fo5176 interaction is conserved among pathosystems. To answer this question, we generated a CLR1 null mutant in the tomato-infecting Fo, Fo14287, and the corresponding *clr1C* complemented line (fig. S8). Similar to Fo5176, tomato plants infected with

Fo1 strains, a higher virulence of $\Delta clr1-1$ mutant compared to WT was observed, while *clr1C* was similar to WT (Fig. 7). These results suggest that CLR1 is not essential for Fo infection, in both Fo5176-Arabidopsis and Fo14287-tomato interactions.

DISCUSSION

Microbes need to loosen and digest the plant CWs to colonize their hosts. As the major and most recalcitrant CW component, cellulose is a key target for a plethora of transcriptionally coordinated microbial CWMPs (15, 34, 38, 39, 63–66). In this work, we studied the

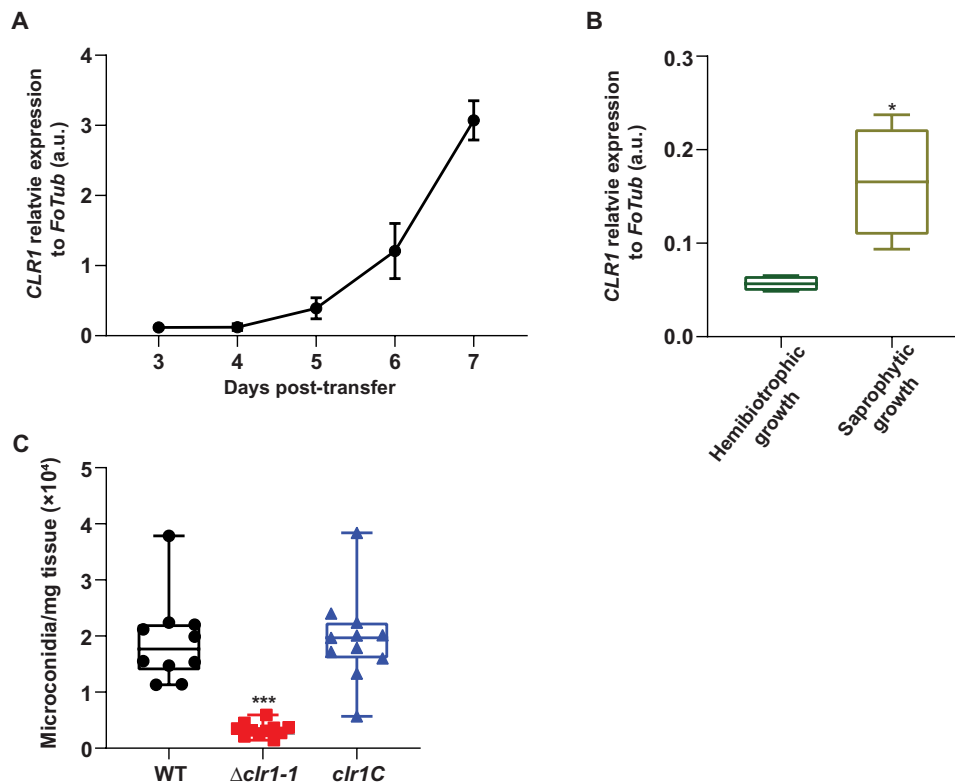


Fig. 6. CLR1 is crucial for *Fo* saprophytic growth and spore production. (A) *CLR1* expression analysis relative to *FoTub* in Arabidopsis-infected roots at different dpt to WT microconidia-containing plates. Values represent means \pm SEM from three biological replicates. (B) *CLR1* expression relative to *FoTub* in WT grown in alive or dead plants for 4 days. The box plots are shown: Centerlines show the medians; box limits indicate the 25th and 75th percentiles; whiskers extend to the minimum and maximum, $N = 4$ biological replicates; Welch's unpaired t test; $*P < 0.05$. (C) Microconidia production of WT, $\Delta clr1-1$, and $clr1C$ in dead aerial tissue of infected Arabidopsis plants. Individual values are shown together with box plots as described above. $N \geq 10$ biological replicates. Asterisks indicate statistical difference relative to WT, Welch's unpaired t test; $***P < 0.001$. a.u., arbitrary units.

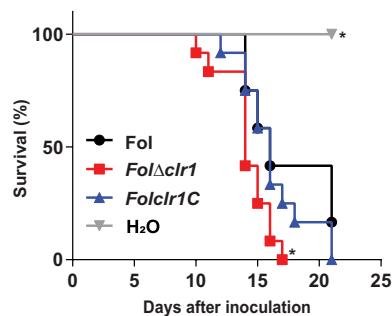


Fig. 7. The lack of CLR1 also increases *Fol4287* pathogenicity in tomato plants. Kaplan-Meier plot showing the survival of tomato plants grown in vermiculite and dip-inoculated or not (H₂O) with *Fol*, *Fol* $\Delta clr1$, or *Fol* $clr1C$ microconidia. $N = 15$ plants from one independent experiment. $*P < 0.05$ versus *Fol* alone according to log-rank test. The experiment was repeated three times with similar results.

function of cellulases in the life cycle of a plant fungal pathogen. The identification and characterization of CLR1 in *Fo* confirm the conservation of this transcription factor as a master regulator of cellulose degradation in ascomycetes (Figs. 1 and 2, G and H, and fig. S3) (8, 38, 39). Our work expands the current knowledge on the role of CLR1 during plant biomass degradation by demonstrating its function in planta. Genes described in *N. crassa* as CLR1 dependent

in cultures with cellulose as the only carbon source behaved similarly in *Fo* during root infection, suggesting that both metabolic situations require similar levels of CWMEs [Fig. 2G; (39)]. Lower gene expression levels of CWMEs were not accompanied by up-regulation of the carbon catabolic repression regulator CRE1 (fig. S5), although further experiments are needed to elucidate its potential implication due to its complex posttranslational regulation. Unexpectedly, loss of CLR1 led to a significant increase in virulence in both the Arabidopsis and tomato pathogenic forms of *Fo* (Fig. 2 and figs. S4 and S7). Although the $\Delta clr1$ mutant is not completely impaired in cellulase secretion (Table 1), our data indicate that *Fo* does not only need their CLR1-dependent cellulases but also benefit from their absence to infect their hosts. More precisely, we show here that $\Delta clr1$ crosses the root epidermal layer and reaches the vascular system of Arabidopsis roots faster, while degrading less crystalline cellulose, than WT (Fig. 2, A to F and H). This indicates that crystalline cellulose degradation is not a requirement for *Fo* to grow through the apoplast of the root layers and that the impairment of $\Delta clr1$ in cellulose degradation is a consequence of the notable decrease in the expression and secretion of most, but not all, cellulolytic enzymes (Figs. 2G and 5B and Table 1).

Our previously reported transcriptomic data indicated that the days 2 and 3 of the root-*Fo*5176 interaction are critical time points for disease development (34). The drastic decrease of sucrose levels detected in infected roots at these time points (Fig. 4, A to C)

suggests that the initial steps of root colonization have an extraordinary impact on plant metabolism. Accordingly, we observed a significant impairment in plant response to $\Delta clr1$ infection at these same time points (Fig. 3A), indicating that the lack of a canonical set of CWDEs stunts the perception of the pathogen by the plant. The identification of cellobiose as a CW degradation product during microbial colonization confirms its predicted but never verified function as DAMP (27). Pretreatment with cellobiose reduced the virulence of the $\Delta clr1$ mutant (Fig. 3B), but its detection in higher amounts in $\Delta clr1$ -infected roots as compared to WT excludes this cellulose degradation product as the main reason for the delay in the perception of $\Delta clr1$ by the plant. The production of cellobiose is not significantly affected in $\Delta clr1$, most probably because it can be originated by xyloglucanases or some of the cellulases still present in the secretome (g12235 or g4892, and g15930 or g12120, respectively; Table 1). Moreover, the high accumulation of cellobiose detected in $\Delta clr1$ -infected roots and the reduced capacity of the mutant to grow on cellobiose as the only carbon source could be explained by a reduction in its uptake, based on the significant down-regulation of the celloextrin transporter *CDT2* in $\Delta clr1$ (Fig. 4F). CDTs have been shown to have a critical role in cellulose and hemicellulose metabolism in *N. crassa* (67). In addition, the significant transcriptional down-regulation of both internal and external β -glucosidases in $\Delta clr1$ might compromise the cellobiose degradation (Fig. 2G) (68). Together with cellobiose, we identified various OGs in Fo-infected roots (Fig. 4, B to E, and fig. S6C). Most of the OGs identified in roots infected with either WT or $\Delta clr1$ were acetylated, which differs from what was reported in leaves infected by the necrotrophic fungus *Botrytis cinerea* (49). Aerial and soil-borne plant pathogens might thus use a different battery of CWDEs to adapt to the different CWs encountered in leaves and roots, with some functional similarities since certain OGs such as GalA₂ox were detected in both infected organs. Acetylated OGs have been shown to impair the activity of some pectinases, eliciting the plant defense response (69, 70). Thus, the reduced amount of GalA₂ox and GalA₄Ac detected in $\Delta clr1$ -infected roots (Fig. 4, D and E) might partially contribute to the delay in fungal perception by the plant.

Plant pathogens modulate their secretome to adapt to the host and to available nutrient sources (8, 71). Together with the decreased amount of cellulases in the $\Delta clr1$ secretome, we found an enrichment of secreted virulence factors, which might partially explain the fact that coinfection with WT does not reduce the hypervirulence of the mutant (fig. S7, A and B). The most enriched protein in the $\Delta clr1$ secretome was a putative cutinase. Cutinases are essential for virulence of aerial plant pathogens (52), where the cuticle is a substantial barrier on the leaf and stem surfaces. In roots, only the root caps have been shown to have a cuticle (72). However, both pathogenic fungi and mutualistic mycorrhizae recruit the fatty acid biosynthesis program to facilitate host invasion. As reported for these microbes (34, 73), we observed an up-regulation of the expression of these fatty acid biosynthesis genes in Fo during Arabidopsis root infection. In addition, cutinases from plant pathogens were shown to cleave suberin *in vitro* (74), a plant compound that prevents the spread of microbial pathogens (75). Because suberin blocks apoplastic transport both at the endodermis and at the root surface (76), the increased amounts of cutinase might explain the ability of $\Delta clr1$ to cross the root epidermal layer and reach the xylem faster than WT (Fig. 2).

We also found a set of peptidases enriched in the $\Delta clr1$ secretome, some of which have been reported to affect host responses by degrading defense-related proteins (56, 77). Among them, fungalysins have been reported to be involved in cleavage of plant chitinases and therefore be essential for the pathogenicity of different fungi, including *Fol* (60, 78). The $\Delta clr1$ mutant also seems to undermine host defense responses by secreting more chitin deacetylases, which should decrease the amount of MAMPs available for plant perception (62). We found that pretreatment with chitin oligomers reduces $\Delta clr1$ virulence to WT levels, implying that not only DAMP but also MAMP perception is severely compromised during $\Delta clr1$ infection. The other group of virulence factors significantly enriched in the $\Delta clr1$ secretome are the pectin and pectate lyases, which have a fundamental role in vascular wilt diseases (54). These enzymes generate unsaturated OGs that might be used efficiently as nutrients by Fo because most OGs detected in the secretomes were saturated. In line with this, the only unsaturated OG identified in the assay, GalA₃Ac-H₂Oox, was less abundant in the $\Delta clr1$ secretome (fig. S6C). We did not find differences in the levels of polygalacturases (PGs) despite the higher levels of saturated OGs observed in infected roots. Most likely, the higher levels of pectin and pectate lyases detected might provide additional substrates for PGs, whose activity would not be a limiting factor in this reaction. The overaccumulation of subtilisin in the $\Delta clr1$ secretome could create more cleavage sites for the PGs by activating type I pectin methyl esterases (79). The lower amount of saturated OGs observed in $\Delta clr1$ -infected compared to WT-infected roots might thus be a consequence of (i) the higher cellulose degradation during WT infection that makes the cellulose-interacting pectin more accessible for deconstruction by pectinases or (ii) the increased capacity of $\Delta clr1$ to uptake and use these OGs. We favor the second hypothesis considering that most pectins are not bound to cellulose (80), although this idea needs to be experimentally confirmed. Overall, the increase in the secretion of different virulence factors might explain the hypervirulence of $\Delta clr1$ (Figs. 2A and 7) and the delay in its perception by the plant at the early stages of infection (Fig. 3A). Delayed host response could also be a consequence of a potential role of CLR1-regulated cellulases as MAMPs, as reported for CWDEs secreted by oomycetes (81), an idea that should be further evaluated.

Sucrose was highly available for Fo at the beginning of its interaction with the root (2 dpt), when Fo is entering the epidermal apoplast (34), while the CW-derived oligomers were not detectable (Fig. 4). At 3 dpt when some hyphae have reached the cortical apoplast [Fig. 2F (34)], sucrose levels had decreased markedly and cellobiose and OGs were detectable, indicating that from 2 to 3 dpt the CW becomes the primary carbon source for the fungus. At this stage, energy acquisition might become limiting in $\Delta clr1$ due to its reduced capacity to degrade cellulose. In this metabolic context, the enrichment in pectin and pectate lyases detected in the $\Delta clr1$ secretome might represent a metabolic adaptation to exploit energy through the alternative carbon source pectin. Moreover, the higher levels of peptidases secreted by $\Delta clr1$ could also provide additional carbon and nitrogen sources to the fungus (82, 83). This hypothesis is supported by the fact that the increase in the expression of virulence factors in $\Delta clr1$ compared to WT was observed during growth in planta and on cellulose but not on carbon-rich axenic medium (Fig. 5, D to F).

Last, the composition of the medium strongly affected conidia production by Fo. A positive role of cellulose in conidia formation

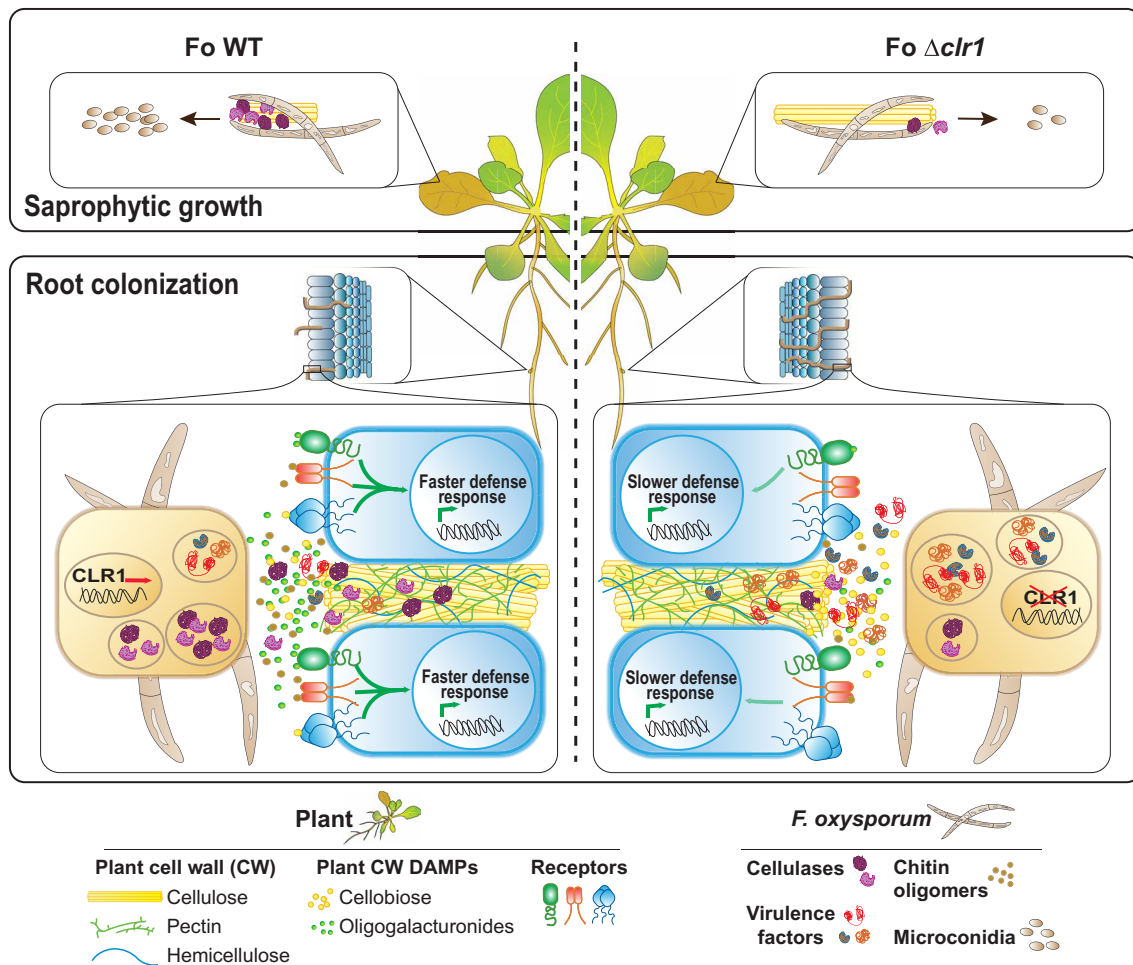


Fig. 8. Model of CLR1 role in the life cycle of *Fo* in planta. Bottom part: During root apoplast colonization, CLR1 is required to degrade and consume the plant cellulose. In its absence, the $\Delta clr1$ mutant secretes more virulence factors and produces less OGs, which are pectin-derived DAMPs. The virulence factors secreted by $\Delta clr1$ also reduce the production of chitin monomers perceived as MAMPs by the plant. Consequently, the host recognizes $\Delta clr1$ less efficiently than WT and $\Delta clr1$ can colonize the xylem faster. Green arrows represent signaling cascade activation; their intensity reflects how much it is triggered. Top part: Once the plant is dead, *Fo* needs CLR1 to use cellulose as carbon source for saprophytic growth and production of microconidia.

was reported previously (84); accordingly, *CLR1* expression was up-regulated starting at 4 dpt, when *Fo* has already entered the xylem (Figs. 2A and 6A), and remained significantly high when the fungus was growing on dead plants compared to alive ones (Fig. 6B). The delay in *CLR1* induction in planta (Fig. 6A) is likely a stealth strategy of *Fo* to avoid cellulose degradation until it is necessary to support the infection cycle. *CLR1* expression seems to prepare the fungal metabolism in advance for the next step in the *Fo* life cycle, i.e., formation of conidia on the decaying plant tissue where cellulose degradation plays a fundamental role in allowing the spread of the fungus to encounter other hosts. We showed that $\Delta clr1$ was severely compromised in asexual reproduction because microconidia formation on dead plants decreased markedly (Fig. 6C). Our data suggest that cellulose degradation is fundamental for the pathogen to fully exploit host resources for the production of dissemination structures.

In conclusion, we show that impairment in cellulose degradation does not pose any obstacles for plant infection by the vascular pathogen *Fo*. We further demonstrate that this organism exhibits an extraordinarily high degree of metabolic plasticity that compensates the decrease in cellulase production during host colonization by

triggering the expression of alternative CWDEs (Fig. 8). However, the deficiency in obtaining energy from cellulose significantly decreases the capacity of the fungus to replicate, disseminate, and invade other hosts. Our findings imply that *CLR1* is highly conserved among ascomycetes because it is vital for saprophytic survival in natural environments. Evolutionary pressure thus makes the use of cellulases imperative for successful completion of the pathogen's life cycle.

MATERIALS AND METHODS

Plant material and growth conditions

A. thaliana ecotype Col-0 and tomato Monika (provided by Syngenta Seeds, Almeria, Spain) were used in the analysis of fungal pathogenicity. Growth conditions were 16-hour light (24°)/8-hour dark cycle at 21°C for all Arabidopsis experiments. In the case of plate experiments, seedlings were grown upright with $1/2$ MS medium (pH adjusted to 5.7 with KOH but without buffering). When the experiment was performed in a hydroponic system, the seeds were germinated on 2-mm foam plugs floating in 330-ml pots on $1/2$ MS + 1% sucrose medium at pH 5.7 adjusted by KOH. The

medium was exchanged 6 days after germination to $1/2$ MS, and seedlings were further grown. Tomato cultivar susceptible cultivar Monika (provided by Syngenta Seeds, Almeria, Spain) was planted in vermiculite and maintained in a growth chamber (28°C; photoperiod 14-hour light/10-hour dark).

Fungal strains and culture conditions

Fo strain 5176 (Fo5176) was originally isolated in Australia from infected *Arabidopsis* plants (41). For tomato infection, we used *Fo* sp. *lycopersici* isolate 4287 (FGSC 9935). The strains were routinely cultured in potato dextrose broth at 28°C with orbital shaking at 170 rpm. Where necessary, the following antibiotics were added to the culture medium: hygromycin B (55 µg/ml), G418 (100 µg/ml), and phleomycin (5.5 µg/ml). For microconidia collection, 3- to 5-day-old cultures were collected by filtration through a nylon filter (Monodur; mesh size, 10 µm). Filtrates were centrifuged at 12,000g for 10 min, and the pellet containing the microconidia was washed using deionized water and resuspended in water to reach the desired concentration.

Identification of CLR1 in *Fusarium* species

Fusarium genes encoding the predicted CLR1 proteins were identified by sequence similarity searches against the *N. crassa* CLR1 (NCU07705) (38) using BLASTp (<http://blast.ncbi.nlm.nih.gov/>). The software CLC Genomic Workbench v.12 was used to perform the comparison analysis of CLR1 sequence in different ascomycetes.

Fungal transformation

As described above, we identified the CLR1 proteins in Fo5176 (FOXB_08021) and Fol4287 (FOXG_08626). Targeted gene deletion of the entire *CLR1* gene in the *Fo5176-pSIX1::GFP* background (33) and the *Fol4287-3XmClover3* genetic backgrounds was performed using the split-marker method (85) with the neomycin resistance cassettes following the protocol previously described (66). For the complementation of the $\Delta clr1$ deletion mutants, a cotransformation with the native *CLR1* in the phleomycin resistance cassette was performed as reported (86). The oligonucleotides used to generate PCR fragments for gene replacement, complementation, or identification of mutants are listed in Table 1. PCRs were routinely performed with the High-Fidelity Template PCR System (Roche Diagnostics, Barcelona, Spain) using an MJ Mini personal thermal cycler (Bio-Rad, Alcobendas, Spain). The amplified flanking sequences were PCR-fused with partially overlapping truncated versions of the neomycin (Neo^r). Transformants were purified by monoconidial isolation (87).

Fungal growth in different carbon sources

Fo5176 was grown on $1/2$ MS medium (Murashige and Skoog medium, Difco). Carbon sources were added to 0.5% (w/v). Conidia were inoculated into 3 ml of liquid medium at 10^6 conidia/ml and grown at 28°C in the dark and shaking (180 rpm), 3 days for sucrose and cellobiose (Fluka) and 7 days for cellulose (SigmaCell, cellulose type 50). For dry weight quantification, after 1-day drying at 60°, the material was weighted. For the nucleic acid extraction, we followed a previous protocol (88). The nucleic acids were quantified by spectrophotometry using NanoDrop.

To analyze the expression of virulence factors in cultures with cellulose, 10^6 conidia/ml were inoculated into 3 ml of liquid medium

with 0.5% (w/v) sucrose and grown for 24 hours at 28°C in the dark and shaking (180 rpm). Then, the cultures were centrifuged at 4000g during 20 min to pellet the hyphae. After three washes with distilled water, the hyphae were resuspended into 3 ml of liquid medium with 0.5% cellulose and grown for 3 days at 28°C in the dark and shaking (180 rpm). Last, the cultures were centrifuged at 4000g for 20 min to collect the hyphae and extract the RNA.

Fungal growth in in vitro stress conditions

Drops containing serial dilution (1×10^7 , 1×10^6 , and 1×10^5) of freshly obtained microconidia were spotted on YPD agar plates supplemented with Congo red (50 µg/ml) or Calcofluor white (40 µg/ml) prepared in 0.5% KOH for testing CW stress as in (89). Minimal medium was used for evaluating growth under nutrient deficiency, 1 M sorbitol was used to test hyperosmotic stress. Plates were incubated at 28°C for 2 days before imaging, except for osmotic stress and Calcofluor white, where the fungi grew for 3 days.

Arabidopsis plant infection assays

Arabidopsis infection assays were performed as described previously (33, 44). In summary, 8-day-old seedlings grown as described above were transplanted to plates with 100 µl of 10^7 microconidia/ml of Fo5176 *pSIX1::GFP*. Under a stereomicroscope, we observe the GFP signal from the fungus specifically when it reaches the host vasculature of the main and/or lateral roots with a clear, central, linear pattern. We count each of the individual GFP-labeled events as an individual fungal vascular penetration of the root vasculature.

The experiment in which the plants were pretreated with 100 µM cellobiose (Fluka, 22150) or chitin (100 µg/ml) (Sigma-Aldrich, C9752) was based on (27). Chitin powder was dissolved in sterile Milli-Q water by vortexing with glass beads, followed by three rounds of the following: 10 min at 60°C, 45-s grinding (frequency, 30/s for 45 s), and another minute at 60°C. Last, we centrifuged the samples for 10 min at 4000g and used the supernatant. Roots of 10-day-old seedlings were treated with cellobiose or chitin for 25 min; hereafter, they were transferred to $1/2$ MS plates where Fo had grown for 3 days. The number of vascular penetrations was monitored as explained above. The experiment to check *CLR1* expression during hemibiotrophic or saprophytic growth was performed using plate infection assay as described above. The dead plant material was obtained by drying 8-day-old seedlings for 1 day at 60°C. The dead plants were transfer to plates with microconidia as it is indicated above.

Tomato plant infection assays

Tomato root infection with *Fol* was performed as previously described by (87). Briefly, 2-week-old seedlings were inoculated with *Fol* by immersing the roots into a fungal microconidia suspension (5×10^5 conidia/ml), planted in vermiculite, and maintained in a growth chamber (28°C; photoperiod 14-hour light/10-hour dark). Plant survival was recorded daily up to 29 days, as previously described (90), calculated by the Kaplan-Meier method, and compared among groups using the log-rank test. All infection assays included 10 plants per treatment.

Confocal microscopy

Plate infection assays were performed as described above (see the “*Arabidopsis* plant infection assays” section). At 3 dpt, images were taken with an inverted Zeiss LSM 780 or LSM 880 Airyscan Axio Observer microscope, using the LD C-Apochromat 40×/1.1 W Korr

M27 objective and Immersol W (Zeiss) between lens and coverslip. Fluorescence marker GFP (fungus) was excited at 488 nm, and emitted fluorescence was detected at 490 to 550 nm. The propidium iodide (PI) (for imaging the stained CWs) was excited at 561 nm, and emitted fluorescence was detected at 600 to 735 nm.

A block solid of $1/2$ MS medium was cut out, and 50 μ l of PI (10 μ M; Sigma-Aldrich) was added to the surface of the block. After 10 min, the liquid soaked in and the seedlings (WT, Δ *clr1-1*, or *clr1C*) were transferred to the $1/2$ MS medium block containing PI. After 5 min of incubation, the agar block containing the seedlings was transferred to a coverslip and imaged at the confocal microscope.

For imaging hyphae at the apoplast of cortical cells, 1×2 tiles, two tiles per root, were performed at the same root area (root differentiated zone). The area between the root epidermis and the root vasculature was covered by a sufficient number of z-stacks (2 μ m). The images were postprocessed and analyzed using the “Orthogonal views” tool of ImageJ (National Institutes of Health, <http://rsb.info.nih.gov/ij>). For the quantification, the number of hyphae that reached the cortical cells per root was counted (average of the hyphae in cortex of the two tiles, 1×2).

Cellulose, OGs, and hexoses and quantification in infected roots

Plate infection assays were performed as indicated above. For cellulose quantification, roots were harvested at 7 dpt and processed as described before to measure the crystalline cellulose (33, 91). To quantify OGs and hexoses, roots collected at different dpt were weighted, covered with 100% ethanol for several days, and then dried using a freeze dryer (Christ, Alpha 2-4). The roots were grinded in water (1 ml) and centrifuged (10 min at 10,000g), and the supernatant was collected to be analyzed via HP-SEC-MS. The analysis was performed as indicated before (49). Briefly, samples were diluted at 1 mg/ml in 50 mM ammonium formate and 0.1% formic acid. Chromatographic separation was performed on the ACQUITY UPLC Protein BEH SEC Column (125 Å, 1.7 μ m, 4.6 mm \times 300 mm; Waters Corporation, Milford, MA, USA). Elution was performed in 50 mM ammonium formate and 0.1% formic acid at a flow rate of 400 liters/min and a column oven temperature of 40°C. The injection volume was set to 10 liters. MS detection was performed in negative mode with the end plate offset set voltage to 500 V, capillary voltage to 4000 V, nebulizer 40 psi, dry gas 8 liters/min, and dry temperature 180°C. Major peaks were annotated following accurate mass annotation, isotopic pattern, and MS/MS analysis, as previously described (49).

Real-time quantitative PCR

Frozen samples were grinded using TissueLyser II (Qiagen) and glass beads. One microgram of total RNA/sample extracted by Isol-RNA lysis reagent (5 PRIME) was used to generate first-strand complementary DNA (cDNA) using Maxima H Minus cDNA Synthesis Master Mix with dsDNase (Thermo Fisher Scientific), following the manufacturer’s instructions. Quantitative PCRs were performed in a LightCycler 480II apparatus (Roche) using Fast SYBR Green Master Mix (Thermo Fisher Scientific) in a 10- μ l reaction. Relative transcript levels were quantified with respect to the reference gene *GAPDH600B* for plants (92) or *Fo β TUB* (*FOXG_06228*) for Fo5176 (33). The $2^{-\Delta\text{CT}}$ method was used to quantify the relative expression of each gene. Primers are indicated in table S1.

Protein identification in Fo5176 secretome

Ten-day-old hydroponically grown seedlings were treated with 20 μ l of 10^7 microconidia/ml of either Fo5176 WT or *clr1*, as described before (34). At 3 dpt, the roots were removed and the liquid medium was collected. We next followed the protocol from (93) with some modifications: To remove big particles present in the medium, we filtered it with a 45- μ m sterile filter (Starlab) before concentration with centricons (Amicon Ultra 3k, Merck Millipore) to 1.5-ml volume. One hundred fifty microliters of this 1.5 ml was sent to proteomic analysis.

For each sample, proteins were precipitated with trichloroacetic acid (Sigma-Aldrich) at a final concentration of 5% and washed twice with cold acetone. The dry pellets were dissolved in a 45- μ l buffer [10 mM tris + 2 mM CaCl_2 (pH 8.2)]. Reduction and alkylation of the proteins was performed by adding 2 mM tris(2-carboxyethyl) phosphine hydrochloride (TCEP) and 15 mM iodoacetamine. After 30 min at 60°C, the samples were cooled to room temperature and 4 μ g of Sequencing Grade Trypsin (Promega) for digestion was added. The digestion was carried out at 37°C for 4 hours. The samples were dried to completeness and resolubilized in 20 μ l of 3% acetonitrile and 0.1% formic acid for liquid chromatography–MS/MS analysis. Before injection, the samples were diluted 1:20 in the same solvent.

MS analysis was performed on Orbitrap Fusion Lumos (Thermo Fisher Scientific) equipped with a Digital PicoView source (New Objective) and coupled to an M-Class UPLC (Waters). Solvent composition at the two channels was 0.1% formic acid for channel A and 0.1% formic acid and 99.9% acetonitrile for channel B. For each sample, 1 μ l of diluted peptides was loaded on the commercial MZ Symmetry C18 Trap Column (100 Å, 5 μ m, 180 μ m \times 20 mm; Waters) followed by nanoEase MZ C18 HSS T3 Column (100 Å, 1.8 μ m, 75 μ m \times 250 mm; Waters). The peptides were eluted at a flow rate of 300 nl/min by a gradient from 5 to 22% B in 80 min, 32% B in 10 min, and 95% B for 10 min. Samples were acquired in a randomized order. The mass spectrometer was operated in data-dependent mode acquiring a full-scan MS spectra [300 to 1500 mass/charge ratio (*m/z*)] at a resolution of 120,000 at 200 *m/z* after accumulation to a target value of 500,000. Data-dependent MS/MS was recorded in the linear ion trap using quadrupole isolation with a window of 0.8 Da and higher-energy collisional dissociation (HCD) fragmentation with 35% fragmentation energy. The ion trap was operated in rapid scan mode with a target value of 10,000 and a maximum injection time of 50 ms. Only precursors with intensity above 5000 were selected for MS/MS, and the maximum cycle time was set to 3 s. Charge state screening was enabled. Singly, unassigned, and charge states higher than seven were rejected. Precursor masses previously selected for MS/MS measurement were excluded from further selection for 20 s, and the exclusion window was set at 10 ppm. The samples were acquired using internal lock mass calibration on *m/z* 371.1012 and 445.1200. The MS proteomics data were handled using the local laboratory information management system (94).

For protein identification and label-free protein quantification, the acquired raw MS data were processed by MaxQuant (version 1.6.2.3), followed by protein identification using the integrated Andromeda search engine (95). Spectra were searched against a provided Fo5176 database (43) concatenated to the Araport database (www.arabidopsis.org/download/index-auto.jsp?dir=%2Fdownload_files%2FSequences%2FAraport11_blastsets, version 2020-06-18), concatenated to its reversed decoyed fasta database and common protein contaminants. Carbamidomethylation of cysteine was set as

fixed modification, while methionine oxidation and N-terminal protein acetylation were set as variables. Enzyme specificity was set to trypsin/P, allowing a minimal peptide length of seven amino acids and a maximum of two missed cleavages. MaxQuant Orbitrap default search settings were used. The maximum false discovery rate was set to 0.01 for peptides and 0.05 for proteins. Label-free quantification was enabled, and a 2-min window for match between runs was applied. In the MaxQuant experimental design template, each file is kept separate in the experimental design to obtain individual quantitative values. Protein fold changes were computed on the basis of intensity values reported in the proteinGroups.txt file. A set of functions implemented in the R package SRMServe (96) was used to filter for proteins with two or more peptides, allowing for a maximum of four missing values, and to normalize the data with a modified robust z -score transformation and to compute P values using the t test with pooled variance. If all measurements of a protein are missing in one of the conditions, a pseudo fold change was computed replacing the missing group average by the mean of 10% smallest protein intensities in that condition.

Fo5176 microconidia production in Arabidopsis

We performed plate infection assays as indicated above. Five days after the plant was dead, we weighed the whole plant and added 1.2 ml of H₂O. The samples were shaken gently for 1 min, and the plant material was removed. The number of microconidia in solution counted with the Thoma cell counting chamber was shown per milligram of dead material.

Statistical analysis

Statistical analyses were performed, and data were plotted using GraphPad Prism 9.0.0 (GraphPad Software Inc.). Each figure legend indicates the statistical analysis that was performed and the level of significance.

SUPPLEMENTARY MATERIALS

Supplementary material for this article is available at <https://science.org/doi/10.1126/sciadv.abl9734>

[View/request a protocol for this paper from Bio-protocol.](#)

REFERENCES AND NOTES

- P. Albersheim, A. G. Darvill, M. A. O'Neill, H. A. Schols, A. G. J. Voragen, in *Progress in Biotechnology*, J. Visser, A. G. J. Voragen, Eds. (Elsevier, 1996), vol. 14, pp. 47–55.
- J. Graça, Suberin: The biopolyester at the frontier of plants. *Front. Chem.* **3**, 62 (2015).
- S. Naseer, Y. Lee, C. Lapierre, R. Franke, C. Nawrath, N. Geldner, Casparian strip diffusion barrier in *Arabidopsis* is made of a lignin polymer without suberin. *Proc. Natl. Acad. Sci. U.S.A.* **109**, 10101–10106 (2012).
- C. T. Anderson, J. J. Kieber, Dynamic construction, perception, and remodeling of plant cell walls. *Annu. Rev. Plant Biol.* **71**, 39–69 (2020).
- D. J. Cosgrove, Plant cell wall extensibility: Connecting plant cell growth with cell wall structure, mechanics, and the action of wall-modifying enzymes. *J. Exp. Bot.* **67**, 463–476 (2016).
- H. Höfte, A. Voxeur, Plant cell walls. *Curr. Biol.* **27**, R865–R870 (2017).
- N. L. Glass, M. Schmoll, J. H. D. Cate, S. Coradetti, Plant cell wall deconstruction by ascomycete fungi. *Annu. Rev. Microbiol.* **67**, 477–498 (2013).
- V. W. Wu, N. Thieme, L. B. Huberman, A. Dietschmann, D. J. Kowbel, J. Lee, S. Calhoun, V. R. Singan, A. Lipzen, Y. Xiong, R. Monti, M. J. Blow, R. C. O'Malley, I. V. Grigoriev, J. P. Benz, N. L. Glass, The regulatory and transcriptional landscape associated with carbon utilization in a filamentous fungus. *Proc. Natl. Acad. Sci. U.S.A.* **117**, 6003–6013 (2020).
- R. Zhang, Functional characterization of cellulose-degrading AA9 lytic polysaccharide monoxygenases and their potential exploitation. *Appl. Microbiol. Biotechnol.* **104**, 3229–3243 (2020).
- A. B. Boraston, D. N. Bolam, H. J. Gilbert, G. J. Davies, Carbohydrate-binding modules: Fine-tuning polysaccharide recognition. *Biochem. J.* **382**, 769–781 (2004).
- B. Henrissat, A. Bairoch, New families in the classification of glycosyl hydrolases based on amino acid sequence similarities. *Biochem. J.* **293**(Pt. 3), 781–788 (1993).
- P. Reignault, O. Valette-Collet, M. Boccard, The importance of fungal pectinolytic enzymes in plant invasion, host adaptability and symptom type. *Eur. J. Plant Pathol.* **120**, 1–11 (2008).
- N. Tang, H. San Clemente, S. Roy, G. Bécard, B. Zhao, C. Roux, A survey of the gene repertoire of *Gigaspora rosea* unravels conserved features among glomeromycota for obligate biotrophy. *Front. Microbiol.* **7**, 233 (2016).
- E. Tisserant, M. Malbreil, A. Kuo, A. Kohler, A. Symeonidi, R. Balestrini, P. Charron, N. Duensing, N. Frei dit Frey, V. Gianinazzi-Pearson, L. B. Gilbert, Y. Handa, J. R. Herr, M. Hiji, R. Koul, M. Kawaguchi, F. Krajinski, P. J. Lammers, F. G. Masclaux, C. Murat, E. Morin, S. Ndikumana, M. Pagni, D. Petitpierre, N. Requena, P. Rosikiewicz, R. Riley, K. Saito, H. S. Clemente, H. Shapiro, D. van Tuinen, G. Bécard, P. Bonfante, U. Paszkowski, Y. Y. Shachar-Hill, G. A. Tuskan, J. P. W. Young, I. R. Sanders, B. Henrissat, S. A. Rensing, I. V. Grigoriev, N. Corradi, C. Roux, F. Martin, Genome of an arbuscular mycorrhizal fungus provides insight into the oldest plant symbiosis. *Proc. Natl. Acad. Sci. U.S.A.* **110**, 20117–20122 (2013).
- K. Hématy, C. Cherk, S. Somerville, Host-pathogen warfare at the plant cell wall. *Curr. Opin. Plant Biol.* **12**, 406–413 (2009).
- W. Underwood, The plant cell wall: A dynamic barrier against pathogen invasion. *Front. Plant Sci.* **3**, 85 (2012).
- C. P. Kubicek, T. L. Starr, N. L. Glass, Plant cell wall-degrading enzymes and their secretion in plant-pathogenic fungi. *Annu. Rev. Phytopathol.* **52**, 427–451 (2014).
- Z. Zhao, H. Liu, C. Wang, J.-R. Xu, Comparative analysis of fungal genomes reveals different plant cell wall degrading capacity in fungi. *BMC Genomics* **14**, 274 (2013).
- M. Kurašin, P. Våljamäe, Processivity of cellobiohydrolases is limited by the substrate. *J. Biol. Chem.* **286**, 169–177 (2011).
- A. D. Pietro, M. P. Madrid, Z. Caracuel, J. Delgado-Jarana, M. I. G. Roncero, *Fusarium oxysporum*: Exploring the molecular arsenal of a vascular wilt fungus. *Mol. Plant Pathol.* **4**, 315–325 (2003).
- N. J. Tonukari, J. S. Scott-Craig, J. D. Walton, The *Cochliobolus carbonum* SNF1 gene is required for cell wall-degrading enzyme expression and virulence on maize. *Plant Cell* **12**, 237–248 (2000).
- T. Boller, Chemoperception of microbial signals in plant cells. *Annu. Rev. Plant Physiol. Plant. Mol. Biol.* **46**, 189–214 (1995).
- A. M. Husaini, A. Sakina, S. R. Cambay, Host-pathogen interaction in *Fusarium oxysporum* infections: Where do we stand? *Mol. Plant Microbe Interact.* **31**, 889–898 (2018).
- S. Hou, Z. Liu, H. Shen, D. Wu, Damage-associated molecular pattern-triggered immunity in plants. *Front. Plant Sci.* **10**, 646 (2019).
- S. Ferrari, D. V. Savatin, F. Sicilia, G. Gramagna, F. Cervone, G. D. Lorenzo, Oligogalacturonides: Plant damage-associated molecular patterns and regulators of growth and development. *Front. Plant Sci.* **4**, 49 (2013).
- A. Voxeur, H. Höfte, Pectin-derived immune elicitors in response to lignin modification in plants. *Proc. Natl. Acad. Sci. U.S.A.* **117**, 4442–4444 (2020).
- C. de Azevedo Souza, S. Li, A. Z. Lin, F. Boutrot, G. Grossmann, C. Zipfel, S. C. Somerville, Cellulose-derived oligomers act as damage-associated molecular patterns and trigger defense-like responses. *Plant Physiol.* **173**, 2383–2398 (2017).
- J. M. Johnson, J. Thürich, E. K. Petutschnig, L. Altschmied, D. Meichsner, I. Sherameti, J. Dindas, A. Mrozinska, C. Paetz, S. S. Scholz, A. C. U. Furch, V. Lipka, R. Hedrich, B. Schneider, A. Svatoš, R. Oelmüller, A poly(a) ribonuclease controls the cellulose-based interaction between *Piriformospora indica* and its host *Arabidopsis*. *Plant Physiol.* **176**, 2496–2514 (2018).
- T. R. Gordon, *Fusarium oxysporum* and the *Fusarium* wilt syndrome. *Annu. Rev. Phytopathol.* **55**, 23–39 (2017).
- C. Hall, R. Heath, D. Guest, The infection process of *Fusarium oxysporum* f.sp. *vasinfectum* in Australian cotton. *Australas. Plant Pathol.* **42**, 1–8 (2013).
- J. Nahalkova, J. Fatehi, C. Olivain, C. Alabouvette, Tomato root colonization by fluorescent-tagged pathogenic and protective strains of *Fusarium oxysporum* in hydroponic culture differs from root colonization in soil. *FEMS Microbiol. Lett.* **286**, 152–157 (2008).
- C. Kesten, A. Menna, C. Sánchez-Rodríguez, Regulation of cellulose synthesis in response to stress. *Curr. Opin. Plant Biol.* **40**, 106–113 (2017).
- C. Kesten, F. M. Gámez-Arjona, A. Menna, S. Scholl, S. Dora, A. I. Huerta, H.-Y. Huang, N. Tintor, T. Kinoshita, M. Rep, M. Krebs, K. Schumacher, C. Sánchez-Rodríguez, Pathogen-induced pH changes regulate the growth-defense balance in plants. *EMBO J.* **38**, e101822 (2019).
- A. Menna, S. Dora, G. Sancho-Andrés, A. Kashyap, M. K. Meena, K. Skłodowski, D. Gasperini, N. S. Coll, C. Sánchez-Rodríguez, A primary cell wall cellulose-dependent defense mechanism against vascular pathogens revealed by time-resolved dual transcriptomics. *BMC Biol.* **19**, 161 (2021).
- R. J. Quinlan, M. D. Sweeney, L. Lo Leggio, H. Otten, J.-C. N. Poulsen, K. S. Johansen, K. B. R. M. Krogh, C. I. Jørgensen, M. Tovborg, A. Anthonsen, T. Tryfona, C. P. Walter, P. Dupree, F. Xu, G. J. Davies, P. H. Walton, Insights into the oxidative degradation

- of cellulose by a copper metalloenzyme that exploits biomass components. *Proc. Natl. Acad. Sci. U.S.A.* **108**, 15079–15084 (2011).
36. W. T. Beeson, C. M. Phillips, J. H. D. Cate, M. A. Marletta, Oxidative cleavage of cellulose by fungal copper-dependent polysaccharide monoxygenases. *J. Am. Chem. Soc.* **134**, 890–892 (2012).
 37. A. R. Stricker, K. Grosstessner-Hain, E. Würleitner, R. L. Mach, Xyr1 (xylanase regulator 1) regulates both the hydrolytic enzyme system and D-xylose metabolism in *Hypocrea jecorina*. *Eukaryot. Cell* **5**, 2128–2137 (2006).
 38. S. T. Coradetti, J. P. Craig, Y. Xiong, T. Shock, C. Tian, N. L. Glass, Conserved and essential transcription factors for cellulase gene expression in ascomycete fungi. *Proc. Natl. Acad. Sci. U.S.A.* **109**, 7397–7402 (2012).
 39. J. P. Craig, S. T. Coradetti, T. L. Starr, N. L. Glass, Direct target network of the *Neurospora crassa* plant cell wall deconstruction regulators CLR-1, CLR-2, and XLR-1. *MBio* **6**, e01452-15 (2015).
 40. S. Beier, W. Hinterdobler, H. Bazafkan, L. Schillinger, M. Schmoll, CLR1 and CLR2 are light dependent regulators of xylanase and pectinase genes in *Trichoderma reesei*. *Fungal Genet. Biol.* **136**, 103315 (2020).
 41. L. F. Thatcher, D. M. Gardiner, K. Kazan, J. M. Manners, A highly conserved effector in *Fusarium oxysporum* is required for full virulence on *Arabidopsis*. *Mol. Plant Microbe Interact.* **25**, 180–190 (2012).
 42. D. Nirmaladevi, M. Venkataramana, R. K. Srivastava, S. R. Uppalapati, V. K. Gupta, T. Yli-Mattila, K. M. Clement Tsui, C. Srinivas, S. R. Niranjana, N. S. Chandra, Molecular phylogeny, pathogenicity and toxigenicity of *Fusarium oxysporum* f. sp. *lycopersici*. *Sci. Rep.* **6**, 21367 (2016).
 43. L. Fokkens, L. Guo, S. Dora, B. Wang, K. Ye, C. Sánchez-Rodríguez, D. Croll, A chromosome-scale genome assembly for the *Fusarium oxysporum* strain Fo5176 To establish a model *Arabidopsis*-fungal pathosystem. *G3* **10**, 3549–3555 (2020).
 44. A. I. Huerta, C. Kesten, A. L. Menna, G. Sancho-Andrés, C. Sanchez-Rodríguez, In-plate quantitative characterization of *Arabidopsis thaliana* susceptibility to the fungal vascular pathogen *Fusarium oxysporum*. *Curr. Protoc. Plant Biol.* **5**, e20113 (2020).
 45. A. F. J. Ram, F. M. Klis, Identification of fungal cell wall mutants using susceptibility assays based on Calcofluor white and Congo red. *Nat. Protoc.* **1**, 2253–2256 (2006).
 46. H. C. van der Does, R. G. E. Duyvesteyn, P. M. Goltstein, C. C. N. van Schie, E. M. M. Manders, B. J. C. Cornelissen, M. Rep, Expression of effector gene SIX1 of *Fusarium oxysporum* requires living plant cells. *Fungal Genet. Biol.* **45**, 1257–1264 (2008).
 47. W. Jonkers, M. Rep, Mutation of *CRE1* in *Fusarium oxysporum* reverts the pathogenicity defects of the *FRP1* deletion mutant. *Mol. Microbiol.* **74**, 1100–1113 (2009).
 48. S. Masachis, D. Segorbe, D. Turrà, M. Leon-Ruiz, U. Fürst, M. El Ghali, G. Leonard, M. S. López-Berges, T. A. Richards, G. Felix, A. Di Pietro, A fungal pathogen secretes plant alkalinizing peptides to increase infection. *Nat. Microbiol.* **1**, 16043 (2016).
 49. A. Voxelor, O. Habrylo, S. Guénin, F. Miart, M.-C. Soulié, C. Rihouey, C. Pau-Roblot, J.-M. Doman, L. Gutierrez, J. Pelloux, G. Mouille, M. Fagard, H. Höfte, S. Vernhettes, Oligogalacturonide production upon *Arabidopsis thaliana*-*Botrytis cinerea* interaction. *Proc. Natl. Acad. Sci. U.S.A.* **116**, 19743–19752 (2019).
 50. M. E. Rauwane, U. V. Ogugua, C. M. Kalu, L. K. Ledwaba, A. A. Woldeamayot, K. Ntshelo, Pathogenicity and virulence factors of *Fusarium graminearum* including factors discovered using next generation sequencing technologies and proteomics. *Microorganisms* **8**, 305 (2020).
 51. M. Andlar, T. Rezić, N. Mardetko, D. Kracher, R. Ludwig, B. Šantek, Lignocellulose degradation: An overview of fungi and fungal enzymes involved in lignocellulose degradation. *Eng. Life Sci.* **18**, 768–778 (2018).
 52. H. Ma, B. Zhang, Y. Gai, X. Sun, K.-R. Chung, H. Li, Cell-wall-degrading enzymes required for virulence in the host selective toxin-producing necrotroph *Alternaria alternata* of citrus. *Front. Microbiol.* **10**, 2514 (2019).
 53. C. A. Cuomo, U. Güldener, J.-R. Xu, F. Trail, B. G. Turgeon, A. Di Pietro, J. D. Walton, L.-J. Ma, S. E. Baker, M. Rep, G. Adam, J. Antoniw, T. Baldwin, S. Calvo, Y.-L. Chang, D. Decaprio, L. R. Gale, S. Gnerre, R. S. Goswami, K. Hammond-Kosack, L. J. Harris, K. Hilburn, J. C. Kennell, S. Kroken, J. K. Magnuson, G. Mannhaupt, E. Mauceli, H.-W. Mewes, R. Mitterbauer, G. Muehlbauer, M. Münsterkötter, D. Nelson, K. O'donnell, T. Ouellet, W. Qi, H. Quesneville, M. I. G. Roncero, K.-Y. Seong, I. V. Tetko, M. Urban, C. Waalwijk, T. J. Ward, J. Yao, B. W. Birren, H. C. Kistler, The *Fusarium graminearum* genome reveals a link between localized polymorphism and pathogen specialization. *Science* **317**, 1400–1402 (2007).
 54. Y. Yang, Y. Zhang, B. Li, X. Yang, Y. Dong, D. Qiu, A *Verticillium dahliae* pectate lyase induces plant immune responses and contributes to virulence. *Front. Plant Sci.* **9**, 1271 (2018).
 55. I. Kars, G. H. Krooshof, L. Wagemakers, R. Joosten, J. A. E. Benen, J. A. L. van Kan, Necrotizing activity of five *Botrytis cinerea* endopolygalacturonases produced in *Pichia pastoris*. *Plant J.* **43**, 213–225 (2005).
 56. M. Monod, S. Capoccia, B. Léchenne, C. Zaugg, M. Holdom, O. Jousson, Secreted proteases from pathogenic fungi. *Int. J. Med. Microbiol.* **292**, 405–419 (2002).
 57. I. E. Cota, R. Troncoso-Rojas, R. Sotelo-Mundo, A. Sánchez-Estrada, M. E. Tiznado-Hernández, Chitinase and β -1,3-glucanase enzymatic activities in response to infection by *Alternaria alternata* evaluated in two stages of development in different tomato fruit varieties. *Sci. Hortic.* **112**, 42–50 (2007).
 58. J. M. Sanz-Martín, J. R. Pacheco-Arjona, V. Bello-Rico, W. A. Vargas, M. Monod, J. M. Diaz-Minguez, M. R. Thon, S. A. Sukno, A highly conserved metalloprotease effector enhances virulence in the maize anthracnose fungus *Colletotrichum graminicola*. *Mol. Plant Pathol.* **17**, 1048–1062 (2016).
 59. B. Ökmen, B. Kemmerich, D. Hilbig, R. Wemhöner, J. Aschenbroich, A. Perrar, P. F. Huesgen, K. Schipper, G. Doehlemann, Dual function of a secreted fungalysin metalloprotease in *Ustilago maydis*. *New Phytol.* **220**, 249–261 (2018).
 60. M. K. Jashni, I. H. M. Dols, Y. Iida, S. Boeren, H. G. Beenen, R. Mehrabi, J. Collemare, P. J. G. M. de Wit, Synergistic action of a metalloprotease and a serine protease from *Fusarium oxysporum* f. sp. *lycopersici* cleaves chitin-binding tomato chitinases, reduces their antifungal activity, and enhances fungal virulence. *Mol. Plant Microbe Interact.* **28**, 996–1008 (2015).
 61. T. A. Naumann, D. T. Wicklow, N. P. J. Price, Identification of a chitinase-modifying protein from *Fusarium verticillioides*: Truncation of a host resistance protein by a fungalysin metalloprotease. *J. Biol. Chem.* **286**, 35358–35366 (2011).
 62. F. Gao, B. S. Zhang, J. H. Zhao, J. F. Huang, P. S. Jia, S. Wang, J. Zhang, J. M. Zhou, H. S. Guo, Deacetylation of chitin oligomers increases virulence in soil-borne fungal pathogens. *Nat. Plants* **5**, 1167–1176 (2019).
 63. F. G. Malinovsky, J. U. Fangel, W. G. T. Willats, The role of the cell wall in plant immunity. *Front. Plant Sci.* **5**, 178 (2014).
 64. H. Liu, S. Zhang, M. A. Schell, T. P. Denny, Pyramiding unmarked deletions in *Ralstonia solanacearum* shows that secreted proteins in addition to plant cell-wall-degrading enzymes contribute to virulence. *Mol. Plant Microbe Interact.* **18**, 1296–1305 (2005).
 65. B. Van Vu, K. Itoh, Q. B. Nguyen, Y. Tosa, H. Nakayashiki, Cellulases belonging to glycoside hydrolase families 6 and 7 contribute to the virulence of *Magnaporthe oryzae*. *Mol. Plant Microbe Interact.* **25**, 1135–1141 (2012).
 66. N. Rispaill, A. Di Pietro, *Fusarium oxysporum* Ste12 controls invasive growth and virulence downstream of the Fmk1 MAPK cascade. *Mol. Plant Microbe Interact.* **22**, 830–839 (2009).
 67. P. Cai, R. Gu, B. Wang, J. Li, L. Wan, C. Tian, Y. Ma, Evidence of a critical role for celldextrin transport 2 (CDT-2) in both cellulose and hemicellulose degradation and utilization in *Neurospora crassa*. *PLoS ONE* **9**, e89330 (2014).
 68. X. Zang, M. Liu, Y. Fan, J. Xu, X. Xu, H. Li, The structural and functional contributions of β -glucosidase-producing microbial communities to cellulose degradation in composting. *Biotechnol. Biofuels* **11**, 51 (2018).
 69. B. Randoux, D. Renard-Merlier, G. Mulard, S. Rossard, F. Duyme, J. Samsen, J. Courtois, R. Durand, P. Reignault, Distinct defenses induced in wheat against powdery mildew by acetylated and nonacetylated oligogalacturonides. *Phytopathology* **100**, 1352–1363 (2010).
 70. G. Pogorelko, V. Lionetti, O. Fursova, R. M. Sundaram, M. Qi, S. A. Whitham, A. J. Bogdanove, D. Bellincampi, O. A. Zabolina, *Arabidopsis* and *Brachypodium* distachyon transgenic plants expressing *Aspergillus nidulans* acetyltransferases have decreased degree of polysaccharide acetylation and increased resistance to pathogens. *Plant Physiol.* **162**, 9–23 (2013).
 71. S. W. McCotter, L. C. Horianopoulos, J. W. Kronstad, Regulation of the fungal secretome. *Curr. Genet.* **62**, 533–545 (2016).
 72. A. Berhin, D. de Bellis, R. B. Franke, R. A. Buono, M. K. Nowack, C. Nawrath, The root cap cuticle: A cell wall structure for seedling establishment and lateral root formation. *Cell* **176**, 1367–1378.e8 (2019).
 73. Y. Jiang, W. Wang, Q. Xie, N. Liu, L. Liu, D. Wang, X. Zhang, C. Yang, X. Chen, D. Tang, E. Wang, Plants transfer lipids to sustain colonization by mutualistic mycorrhizal and parasitic fungi. *Science* **356**, 1172–1175 (2017).
 74. R. Jabloun, M. Khalil, I. E. Ben Moussa, A.-M. Simao-Beauvoir, S. Lerat, R. Brzezinski, C. Beaulieu, Enzymatic degradation of *p*-nitrophenyl esters, Polyethylene terephthalate, cutin, and suberin by Sub1, a suberinase encoded by the plant pathogen *Streptomyces scabies*. *Microbes Environ.* **35**, ME19086 (2020).
 75. A. Kashyap, M. Planas-Marquès, M. Capellades, M. Valls, N. S. Coll, Blocking intruders: Inducible physico-chemical barriers against plant vascular wilt pathogens. *J. Exp. Bot.* **72**, 184–198 (2021).
 76. I. Baxter, P. S. Hosmani, A. Rus, B. Lahner, J. O. Borevitz, B. Muthukumar, M. V. Micklebart, L. Schreiber, R. B. Franke, D. E. Salt, Root suberin forms an extracellular barrier that affects water relations and mineral nutrition in *Arabidopsis*. *PLoS Genet.* **5**, e1000492 (2009).
 77. S. Gottwald, B. Samans, S. Lück, W. Friedt, Jasmonate and ethylene dependent defence gene expression and suppression of fungal virulence factors: Two essential mechanisms of *Fusarium* head blight resistance in wheat? *BMC Genomics* **13**, 369 (2012).
 78. T. A. Naumann, D. T. Wicklow, Chitinase modifying proteins from phylogenetically distinct lineages of Brassica pathogens. *Physiol. Mol. Plant Pathol.* **82**, 1–9 (2013).

79. F. Sénéchal, L. Graff, O. Surcouf, P. Marcelo, C. Rayon, S. Bouton, A. Mareck, G. Mouille, A. Stintzi, H. Höfte, P. Lerouge, A. Schaller, J. Pelloux, Arabidopsis PECTIN METHYLESTERASE17 is co-expressed with and processed by SBT3.5, a subtilisin-like serine protease. *Ann. Bot.* **114**, 1161–1175 (2014).
80. M. A. Atmodjo, Z. Hao, D. Mohnen, Evolving views of pectin biosynthesis. *Annu. Rev. Plant Biol.* **64**, 747–779 (2013).
81. Z. Ma, T. Song, L. Zhu, W. Ye, Y. Wang, Y. Shao, S. Dong, Z. Zhang, D. Dou, X. Zheng, B. M. Tyler, Y. Wang, A *Phytophthora sojae* glycoside hydrolase 12 protein is a major virulence factor during soybean infection and is recognized as a PAMP. *Plant Cell* **27**, 2057–2072 (2015).
82. R. G. T. Lowe, O. McCorkelle, M. Bleackley, C. Collins, P. Faou, S. Mathivanan, M. Anderson, Extracellular peptidases of the cereal pathogen *Fusarium graminearum*. *Front. Plant Sci.* **6**, 962 (2015).
83. L. Huang, L. Dong, B. Wang, L. Pan, The transcription factor PrtT and its target protease profiles in *Aspergillus niger* are negatively regulated by carbon sources. *Biotechnol. Lett.* **42**, 613–624 (2020).
84. R. D. Moura, L. A. M. de Castro, M. P. Culik, A. A. R. Fernandes, P. M. B. Fernandes, J. A. Ventura, Culture medium for improved production of conidia for identification and systematic studies of *Fusarium* pathogens. *J. Microbiol. Methods* **173**, 105915 (2020).
85. N. L. Catlett, B.-N. Lee, O. C. Yoder, B. Gillian Turgeon, Split-marker recombination for efficient targeted deletion of fungal genes. *Fungal Genet. Rep.* **50**, 9–11 (2003).
86. M. S. López-Berges, N. Rispail, R. C. Prados-Rosales, A. Di Pietro, A nitrogen response pathway regulates virulence functions in *Fusarium oxysporum* via the protein kinase TOR and the bZIP protein MeaB. *Plant Cell* **22**, 2459–2475 (2010).
87. A. Di Pietro, M. I. Roncero, Cloning, expression, and role in pathogenicity of *pg1* encoding the major extracellular endopolysaccharuronase of the vascular wilt pathogen *Fusarium oxysporum*. *Mol. Plant Microbe Interact.* **11**, 91–98 (1998).
88. U. Raeder, P. Broda, Rapid preparation of DNA from filamentous fungi. *Letts. Appl. Microbiol.* **1**, 17–20 (1985).
89. D. Segorbe, A. Di Pietro, E. Pérez-Nadales, D. Turrà, Three *Fusarium oxysporum* mitogen-activated protein kinases (MAPKs) have distinct and complementary roles in stress adaptation and cross-kingdom pathogenicity. *Mol. Plant Pathol.* **18**, 912–924 (2017).
90. M. S. López-Berges, J. Capilla, D. Turrà, L. Schafferer, S. Matthijs, C. Jöchl, P. Cornelis, J. Guarro, H. Haas, A. Di Pietro, HapX-mediated iron homeostasis is essential for rhizosphere competence and virulence of the soilborne pathogen *Fusarium oxysporum*. *Plant Cell* **24**, 3805–3822 (2012).
91. A. Menna, M. Fischer-Stettler, B. Pfister, G. S. Andrés, D. Holbrook-Smith, C. Sánchez-Rodríguez, Single-run HPLC quantification of plant cell wall monosaccharides. *Bio Protoc.* **10**, e3546 (2020).
92. T. Czechowski, M. Stitt, T. Altmann, M. K. Udvardi, Genome-wide identification and testing of superior reference genes for transcript normalization in Arabidopsis. *Plant Physiol.* **139**, 5–17 (2005).
93. T. Li, Y. Wu, Y. Wang, H. Gao, V. K. Gupta, X. Duan, H. Qu, Y. Jiang, Secretome Profiling reveals virulence-associated proteins of *Fusarium proliferatum* during interaction with banana fruit. *Biomolecules* **9**, 246 (2019).
94. C. Türker, F. Akal, D. Joho, C. Panse, S. Barkow-Oesterreicher, H. Rehrauer, R. Schlapbach, B-Fabric: the Swiss Army Knife for life sciences, in *EDBT '10: Proceedings of the 13th International Conference on Extending Database Technology* (Association for Computing Machinery, 2010), pp. 717–720.
95. J. Cox, M. Mann, MaxQuant enables high peptide identification rates, individualized p.p.b.-range mass accuracies and proteome-wide protein quantification. *Nat. Biotechnol.* **26**, 1367–1372 (2008).
96. W. Witold, J. Grossmann, C. Panse, SRMServe—R-Package to Report Quantitative Mass Spectrometry Data (2018); <http://github.com/protViz/SRMServe>.
97. Y. Perez-Riverol, J. Bai, C. Bandla, D. Garcia-Seisdedos, S. Hewapathirana, S. Kamatchinathan, D. J. Kundu, A. Prakash, A. Frericks-Zipper, M. Eisenacher, M. Walzer, S. Wang, A. Brazma, J. A. Vizcaino, The PRIDE database resources in 2022: A hub for mass spectrometry-based proteomics evidences. *Nucleic Acids Res.* **50**, D543–D552 (2022).

Acknowledgments: We thank all members of the Plant Cell Biology laboratory at ETHZ, especially A. Huerta, C. Kesten, O. Terret, and A. Menna, for technical support and fruitful scientific discussion. We are also very grateful to N. Geldner (UNIL) for fruitful scientific discussions and to P. Nanni and L. Kunz (Functional Genomics Center Zürich, FGCZ) for technical support during the generation and analysis of the proteomic data. We thank the ScopeM (ETH Zurich) for their service in the confocal microscopy. **Funding:** The work described in this paper was supported by the Swiss National Foundation to C.S.-R. (SNF 310030_184769 to S.D. and G.S.-A.), the Vontobel Foundation to F.M.G.-A. and C.S.-R., and the Spanish Ministerio de Ciencia e Innovación (MICINN PID2019-108045RB-I00) to A.D.P. S.V. was supported by Marie Curie ITN FUNGIBRAIN (FP7-PEOPLE-ITN-607963), and A.V. was supported by a National Research Institute for Agriculture, Food and Environment tenure track grant. **Author contributions:** Conceptualization: C.S.-R. Methodology: F.M.G.-A., S.V., A.V., S.D., and J.C.M. Investigation: F.M.G.-A., S.V., A.V., S.D., S.M., G.S.-A., and J.C.M. Visualization: F.M.G.-A., S.V., A.V., S.D., G.S.-A., and J.C.M. Supervision: C.S.-R. and A.D.P. Writing—original draft: F.M.G.-A. and C.S.-R. Writing—review and editing: F.M.G.-A., S.V., A.V., S.D., J.C.M., A.D.P., and C.S.-R. **Competing interests:** The authors declare that they have no competing interests. **Data and materials availability:** All data needed to evaluate the conclusions in the paper are present in the paper and/or the Supplementary Materials. A provided Fo5176 database (43) was used to find the sequence of genes of interest. The mass spectrometry proteomics data have been deposited to the ProteomeXchange Consortium via the PRIDE (97) partner repository with the dataset identifier PXD031137.

Submitted 26 August 2021

Accepted 3 March 2022

Published 20 April 2022

10.1126/sciadv.abl9734

Impairment of the cellulose degradation machinery enhances *Fusarium oxysporum* virulence but limits its reproductive fitness

Francisco M. Gámez-ArjonaStefania VitaleAline VoxeurSusanne DoraSascha MüllerGloria Sancho-AndrésJuan Carlos MontesinosAntonio Di PietroClara Sánchez-Rodríguez

Sci. Adv., 8 (16), eabl9734. • DOI: 10.1126/sciadv.abl9734

View the article online

<https://www.science.org/doi/10.1126/sciadv.abl9734>

Permissions

<https://www.science.org/help/reprints-and-permissions>

Use of this article is subject to the [Terms of service](#)

Science Advances (ISSN) is published by the American Association for the Advancement of Science. 1200 New York Avenue NW, Washington, DC 20005. The title *Science Advances* is a registered trademark of AAAS.

Copyright © 2022 The Authors, some rights reserved; exclusive licensee American Association for the Advancement of Science. No claim to original U.S. Government Works. Distributed under a Creative Commons Attribution NonCommercial License 4.0 (CC BY-NC).